CERAMIZATION OF WOODS INTO POROUS FERRITES AND

THEIR MAGNETIC PROPERTIES

SIA CHEE KIONG

DOCTOR OF ENGINEERING
in
FRONTIER MATERIALS

NAGOYA INSTITUTE OF TECHNOLOGY

JAPAN
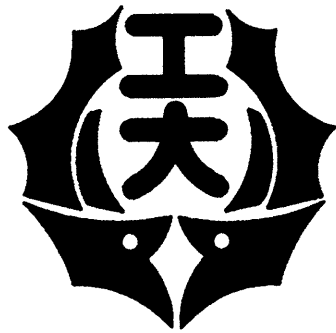
MARCH 2011

論文題目

木材からのフェライト多孔体へのセラミックス化とその磁気的性質

未来材料創成工学専攻博士後期課程

シア　チー　キョン

名古屋工業大学

セラミックス基盤工学研究センター

日本

2011 年 3 月

論文要旨： 木材をテンプレートとして、フェライト前駆体溶液を含浸し、そのまま焼成することにより、セラミックス化を行い、木材の構造を有するフェライト多孔体（フェライト化木）を作製した。原料木材としては、主に、仮導管がハニカム状に並んだ針葉樹（杉材）を用い、組成としては、Ni-Zn フェライト、Mn-Zn フェライトおよび Ba フェライトに関して検討を行った。そして、原料木材の前処理条件、前駆体溶液の調製条件、焼成条件等について、最適作製条件を見出した。えられた試料は、元の木材組織の細胞壁部分が、そのまま面状に焼結してハニカム構造のフェライトへとセラミックス化し、一次元細孔が配向した気孔構造を示した。そのハニカム面の厚みは 1～2 μm で、フェライト粒子 1 ないし数個が焼結して構成されていた。

　フェライト化木の磁気的性質としては、磁気ヒステリシス、透磁率の周波数特性、反射損失を測定した。また、緻密質焼結フェライト、ポリマー複合体および通常の気孔形成剤によるフェライト多孔体との比較を行った。特に Ni-Zn フェライト化木に特徴的な性質として、一次元細孔の方向に垂直方向と平行方向で、磁気的性質が変化することがわかった。磁場が一次元細孔に平行方向に加えられた場合には磁化しやすく、磁化曲線はより急激に飽和磁化に到達し、また、保持力は小さくなった。これらの結果は、フェライト薄膜に見られる薄膜に垂直方向と平行方向における磁気異方性の特徴と一致し、フェライト化木はフェライト薄膜がハニカム状に並んだ多層構造体とみなしてよいと考えられた。また、透磁率は、緻密質焼結フェライトに比べ、高周波数側での低下が小さく、フェライト薄膜に観測されているスヌーク則からのずれと同様な効果が起きていると考えられた。さらに、ギガヘルツ帯で反射損失のピークも小さいながら確認され、フェライト化木の高周波数域における電波吸収体としての利用の可能性が示唆された。

ABSTRACT

Ferrite woods were prepared by ceramizations of woods. The wood templates were infiltrated by precursor solution and sintered. The compositions of the NiZn ferrite, MnZn ferrite and Ba ferrite with 1 directional pore orientation like cedar microstructure which is tracheid line up into honeycomb microstructures was examined. The optimum preparations conditions of ferrite wood were determined by considered the template treatment, precursor solutions preparations and the sintering conditions. The cell walls of the original wood become a ferrite layered ceramic in honeycomb structure with one-dimensional pore orientations. The honeycomb was about 1 - 2μm, was configured with one or few layer of grains.

The magnetic properties of ferrite wood such as magnetic hyteresis, the frequency dependence of permeability and return loss was measured. Dense ferrite, compressed powder and conventional porous ferrites that bonded with polymer were also prepared and the magnetic properties were also examined. As results, the ferrite woods show the magnetic shape anisotropy which is in parallel directions of pores orientations was easier to magnetize compared with perpendicular directions of pores orientations. The ferrite wood was regarded multilayered structure that lined up into honeycomb shape. This magnetic shape anisotropy phenomenon is similar with thin film tendency that might exceed the Snoek's limit. Furthermore, small peak of reflection loss is observed in Gigahertz regions. Therefore possibility of utilization of ferrite woods as the wave absorber in the high frequency regions was suggested.

LIST OF PUBLICATIONS

JOURNALS

[1]   Preparation of Porous Ni-Zn Ferrite Using Wood Templates
       C.K.Sia, M. Kuwahara, H. Hibino, N. Adachi, T.Ota
       Transactions of the Materials Research Society of Japan, 34[1] 105-108 (2009)

[2]   Preparation and Magnetic Properties of Porous Mn-Zn ferrite from wood
       Template.
       Sia Chee Kiong, Daimu Mutou, Nobuyasu Adachi, Toshitaka Ota
       Journal of the Australian Ceramic Society, 45[2] 34- 39 (2009)

[3]   The Magnetic Properties of Porous Ni-Zn Ferrite Prepared from Wood
       Templates
       Chee Kiong Sia, Yuji Sasaki, Nobuyasu Adachi, Toshitaka Ota
       Journal of the Ceramic Society of Japan 117[9] 958-960 (2009)

[4]   Porous Ba Ferrite Prepared from Wood Template
       Nobuyasu Adachi, Masayuki Kuwahara, **Chee Kiong Sia** and Toshitaka Ota
       Materials 2[4], 1923-1928 (2009)

[5]   Magnetic Properties of NiZn ferrite woods at High electro-Magnetic Field.
       Chee Kiong Sia (In preparations)

TABLE OF CONTENTS

CHAPTER 1

INTRODUCTION

1.1 Ceramizations of Wood

Wood has unique microstructures. It has pores that for water transportation purposes by capillary action. Both hard wood and soft wood are contained of elongated tubular cells aligned with the axis of the tree trunk [1]. Some of wood have a big pores and some of it have small pores (micro-size). It depends of the type, age of wood. The wood template was originally containing the organic composition such as gums, troplones, fats and fatty acids [2], and mostly Carbon. Chemically, the major constituents of wood are 50% carbon, 44% Oxygen, 6% hydrogen and 1% trace element [17]. Ceramizations of woods is based on the impregnation of a cellular structure with a ceramic suspension or precursor solution in order to produce a macroporous ceramic exhibiting the same morphology as the original porous material [3]. Since last decade, some researcher was interested in ceramization of wood due to the special structure of wood. According to Andre R. Studart et. al. (2006) the ceramization of wood, SiC Wood was first introduced by T. Ota et al (1995). Since after the study was increased by produce different type of ceramic woods. Researchers were used wood as templates to prepared the ceramics such as Titania[4,5], Si and SiC, [6,7] SiC [8,9,10], Alumina[11], Zirconia[12], Iron Oxide [13]. Several types of woods were also used as a template for the ceramization process. Among the woods are rattan [11], pine [11, 13], paulownia [13], Fir [13], Bamboo [7, 14], Mango tree [6] and etc was used. The characterizations of each ceramic wood were examined. Thus ceramic wood materials theirs own

properties and the most important is the 1 D nano/ micro structure that might be implemented in variety of applications such as thermal and/or sound insulation, absorption, and filtration and as catalysts.

According to [3] had stated five techniques used for produce macroporous ceramic namely polymer replica, wood replica, sacrificial template, direct foaming with surfactants and direct foaming with particles.
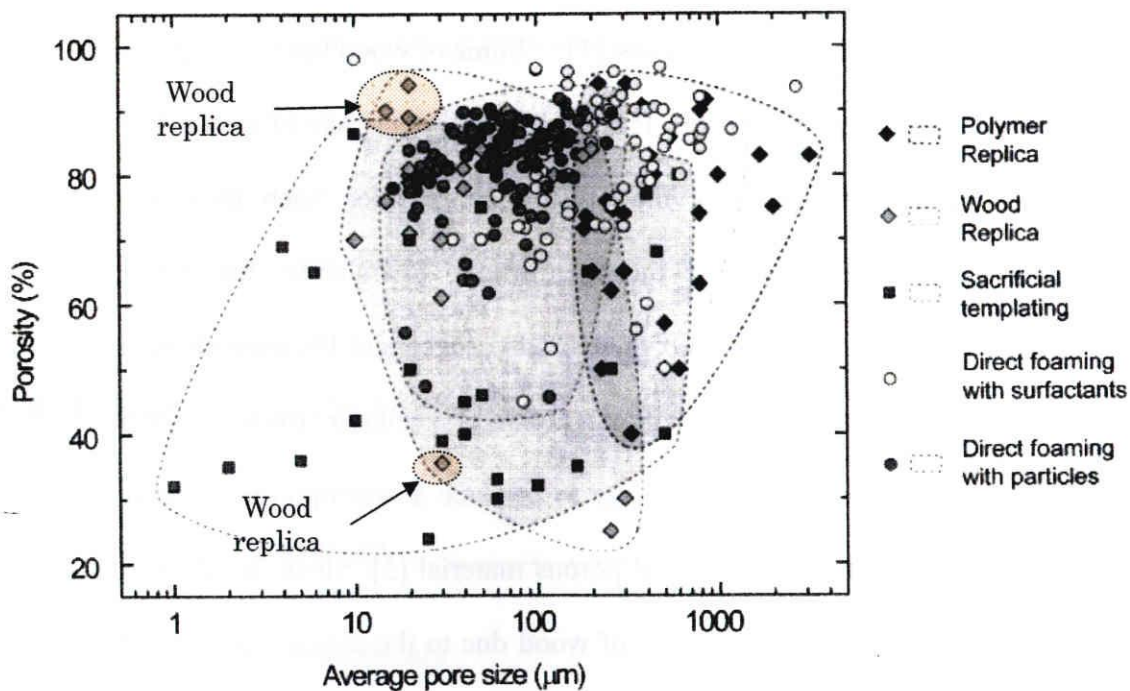
Figure 1.1 Typical porosity and average pore size achieved via various methods [3].

Wood replica among the technique that able to produce high porosity (more than 80%) with small pores sizes (almost 10μm) (figure 1.1). Compared with direct foaming method, the researchers had produced the highest porosity among all the techniques with comparable pores size with wood replica, but it has random distributed pores.

Thus wood replica technique shows the very high porosity and small pores sizes. That means, the walls that construct the pores are very thin. But the interests are

carrying out due to the pores that aligned in one direction. Instead of that reason, the wood replica approach has advantages of the porosity control and pore sizes control. Refer to the figure 1.1, its shows that, the ceramic product from wood replica technique have big ranges of porosity (approximately 30 – 90%). This is because pores sizes were of ceramic wood can be determined by the shrinkages of the template pores. As mentioned, the woods have various sizes of pores depended to the type and the age of the wood.

1.2   Ferrites

1.2.1   Spinel ferrite

In spinel ferrites, the relatively large oxygen anions form a cubic close packing with ½ of the octahedral and ⅛ of the tetrahedral interstitial sites occupied by metal ions (figure 1.2). The distribution of cations over A- and B-sites is determined by their ionic radius, electronic configurations and electrostatic energy in the spinel lattice. Cations like Zn^{2+} and Cd^{2+}, show a marked preference for the A sites, thus their spinels are obtained with a formula $Me^{2+}[Fe^{3+}_2]O_4$, where the Fe^{3+} ions between brackets are on the B-sites. When cations have stronger B-site preference than Fe^{3+}, as is the case for Mn^{2+}, Ni^{2+} and Co^{2+}, Fe^{3+} can occupy A-sites to form inverse spinels, denoted as $Fe^{3+}[Me^{2+}Fe^{3+}]O_4$. [15]
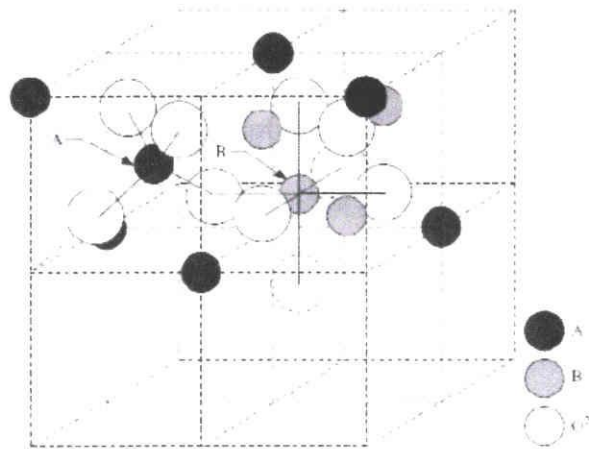
Figure 1.2   Spinel structure A and B represent tetrahedral and octahedral sites

respectively. Adapted from [15]

1.2.2   Hexagonal ferrite

4 types of hexagonal ferrites are distinguishe and indicated as M, W, Y and Z. It was categories by the ratio of $(BaO+MeO)/Fe_2O_3$.

The M type Ba-ferrite have a composition ration of 1:6 of $(BaO+MeO)/Fe_2O_3$[15]. The elementary unit cell contains 10 oxygen layers, sequentially constructed from 4 blocks, S (spinel), R (Hexagonal), S* and R*. S* and R* have equivalent atomic arrangements as S and R, but rotated 180° about c axis with respect to S and R. S and S* block consists of two O^{2-} layers; while R and R* block contains three O^{2-} layers, with one oxygen site in the middle layer substitute by Ba^{2+} ion [15,50,51]. Figure 1.3 shows the structure of M type $BaFe_{12}O_{19}$. In the figure the arrows indicate the spin orientations.

4
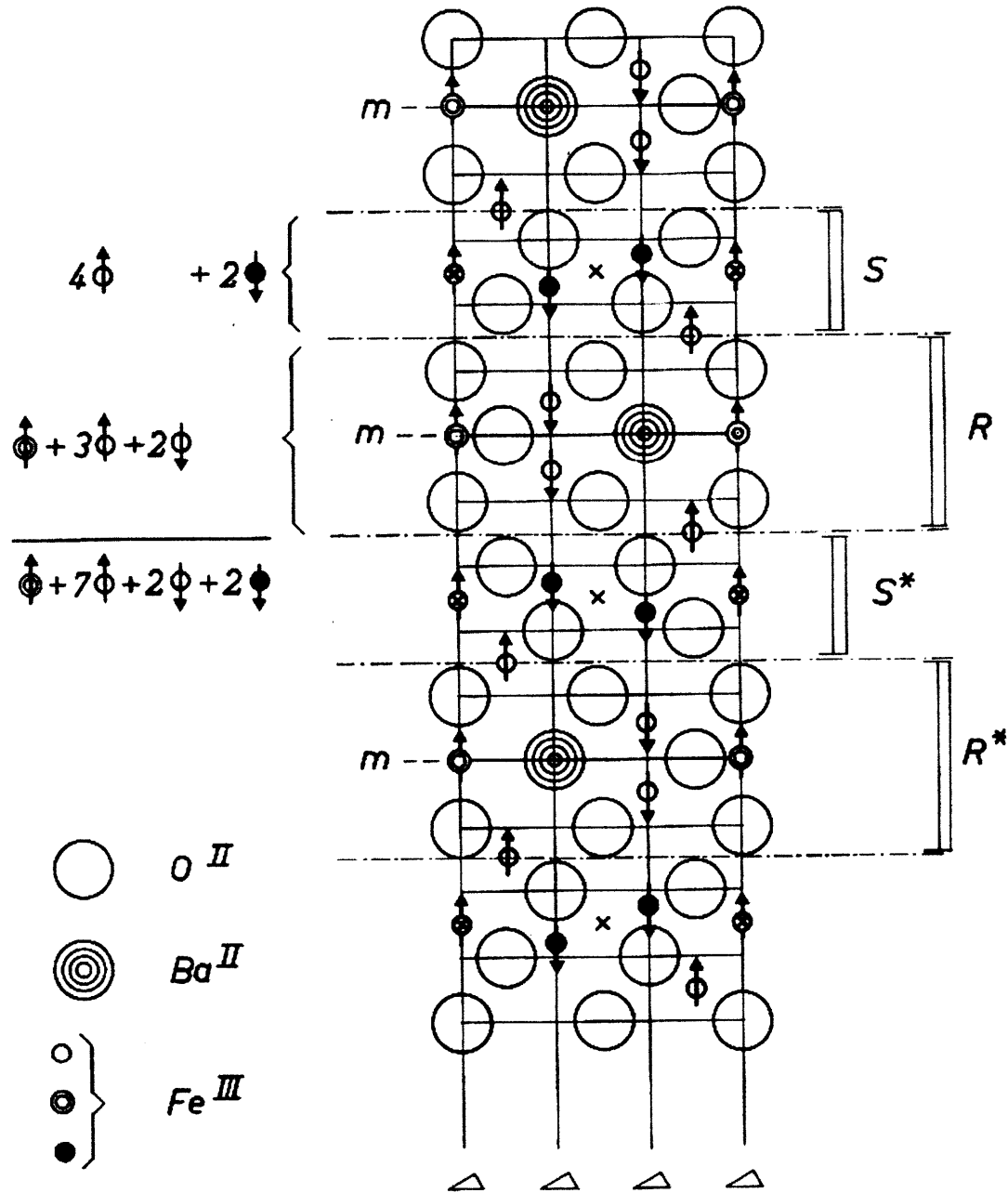
$$M = Ba\,Fe_{12}O_{19}$$

Figure 1.3 structure of M type $BaFe_{12}O_{19}$. Adapted from [16]

1.2.3 Magnetism

Five categories (diamagnetism, paramagnetism, ferromagnetism, anti-

ferromagnetism, and ferrimagnetism) of magnetism are classified into all materials which are depending on their bulk magnetic susceptibility. One of the factor material might change the magnetism behavior ferromagnetic or a ferrimagnetic material is the reversible point above which it becomes paramagnetic at certain temperature depended to the type of the element known as Curie temperature. In order to fulfill the desired constrain (resistivity, dielectric loss, Curie temperature, magnetic permeability etc) more than 1 element are needed.

The comparison of the permeability via hysteresis loop can be concluded in figure 1.4.
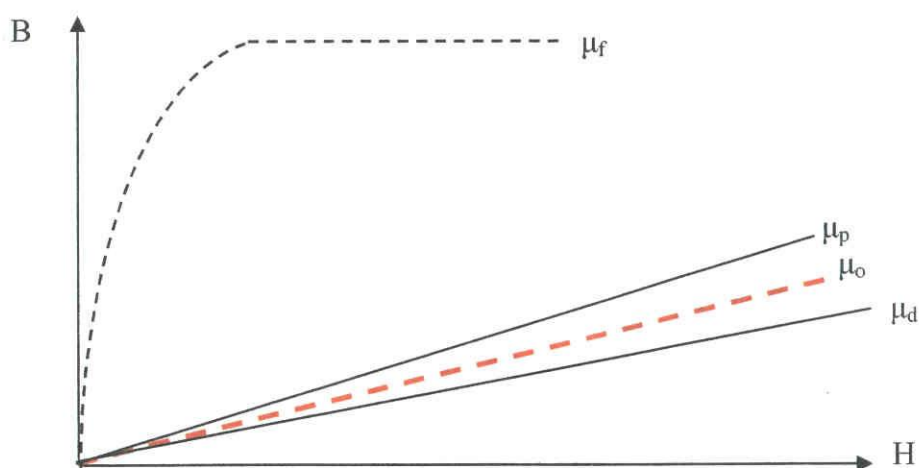
Figure1.4 The comparison of permeability for ferromagnetism μ_f, paramagnetism μ_p, Free space/ Air μ_o, and Diamagnetism μ_d

The Diamagnetism μ_o are the behaviors that have the value of the permeability lower than free space / air. The magnetic materials have a higher permeability than air. But most of the magnetic materials are frequency dependent which is drop at the higher frequency. Some of thus material might have a diamagnetism behavior at higher frequency. This phenomenon discussed in the next sections.

The compound of mixed oxide also known as ferrite, own the ferrimagnetic behavior. For this ferrimagnetic behavior it has a large and positive susceptibility, functioned by the applied field and microstructure dependent. Table 1.1 shows the summarization of ferrimagnetism behavior.

Table 1.1 The summarization of ferrimagnetism behavior

Magnetism	Susceptibility	Atomic/ magnetic behavior	
Ferrimagnetism	Large and positive, function of applied field, microstructure dependent.	Atoms have anti-parallel aligned magnetic moments.	

Ferromagnetism have behavior occurred because the atom due to the entire atom have a parallel aligned magnetic moment meanwhile for ferrimagnetism some of the atom ha anti- parallel aligned magnetic moment. Because of this reason the ferrimagnetism behavior have a lower magnetization compared with ferromagnetism. Those 2 behaviors have a similarity susceptibility which is microstructure dependent. Spinel ferrites have ferrimagnetisms properties;

1.2.4   Permeability of Ni-Zn ferrite

Figure 1.5 shows the frequency dependence of complex permeability (real and imaginary) of $Ni_\delta Zn_{1-\delta}Fe_2O_4$ with different value of δ. The highlighted curve indicated the limits of the real permeability and also known as Snoeks limits. Recently many researchers have developed a new technique, conditions in order to improve the

permeability at the higher frequency.
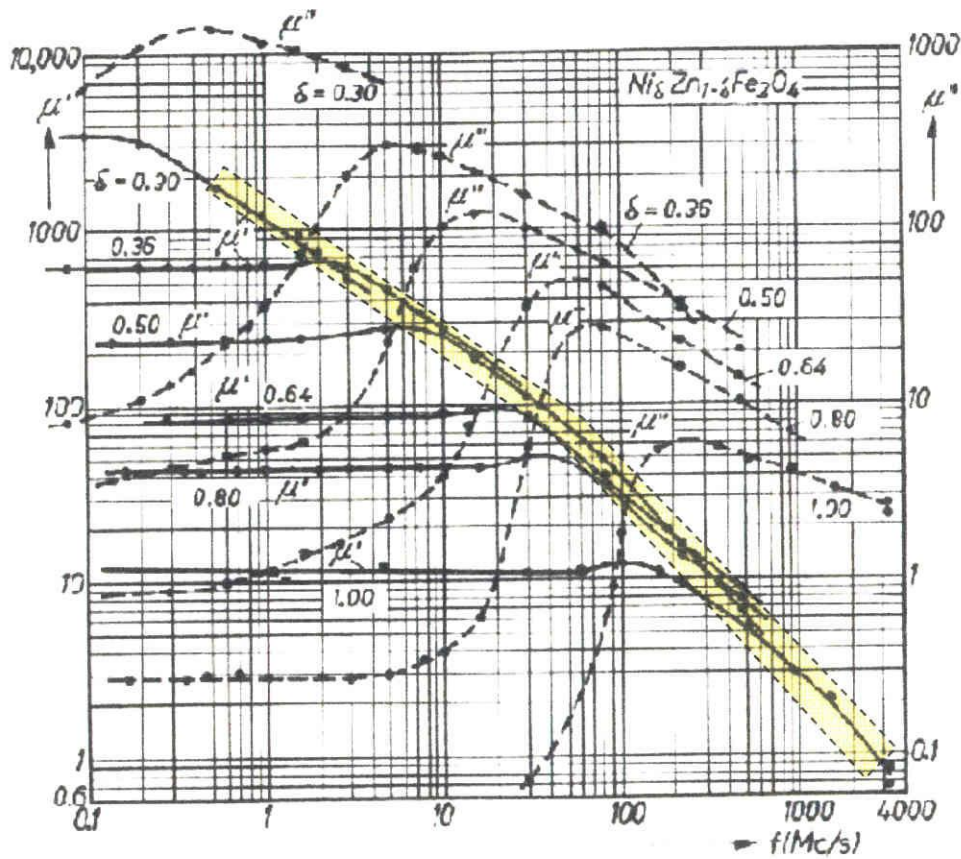
Figure 1.5 Frequency dependence of the real and imaginary parts of the permeability, μ'
and μ" of $Ni_\delta Zn_{1-\delta} Fe_2O_4$. Adapted from [16]

The difficulties are, at the higher frequency regions, the permeability is lower.
Meanwhile, the obtained thus curve (fig 1.6) the specimens are high density. What will
happen if the densities are reduced? Figure 1.6 shows the Ni-Ferrite permeability curve
at various densities. The figure indicated the peak was shifted to the higher frequency.

According to the J. Smith and H.P.J.Wijn, the dispersion frequency drops
continuously with increasing density. The figure also indicates for high density $NiFe_2O_4$
at higher frequency, the real permeability was showed the diamagnetism behavior which
is lower than that air permeability, μ'< 1 or (μ'-1) < 0. But for lower density $NiFe_2O_4$
have a better frequency range than higher density $NiFe_2O_4$. The reason is because of the

lowered porosity (high density) caused less internal shape anisotropy and in higher rotational permeability and a lower ferromagnetic resonance frequency.
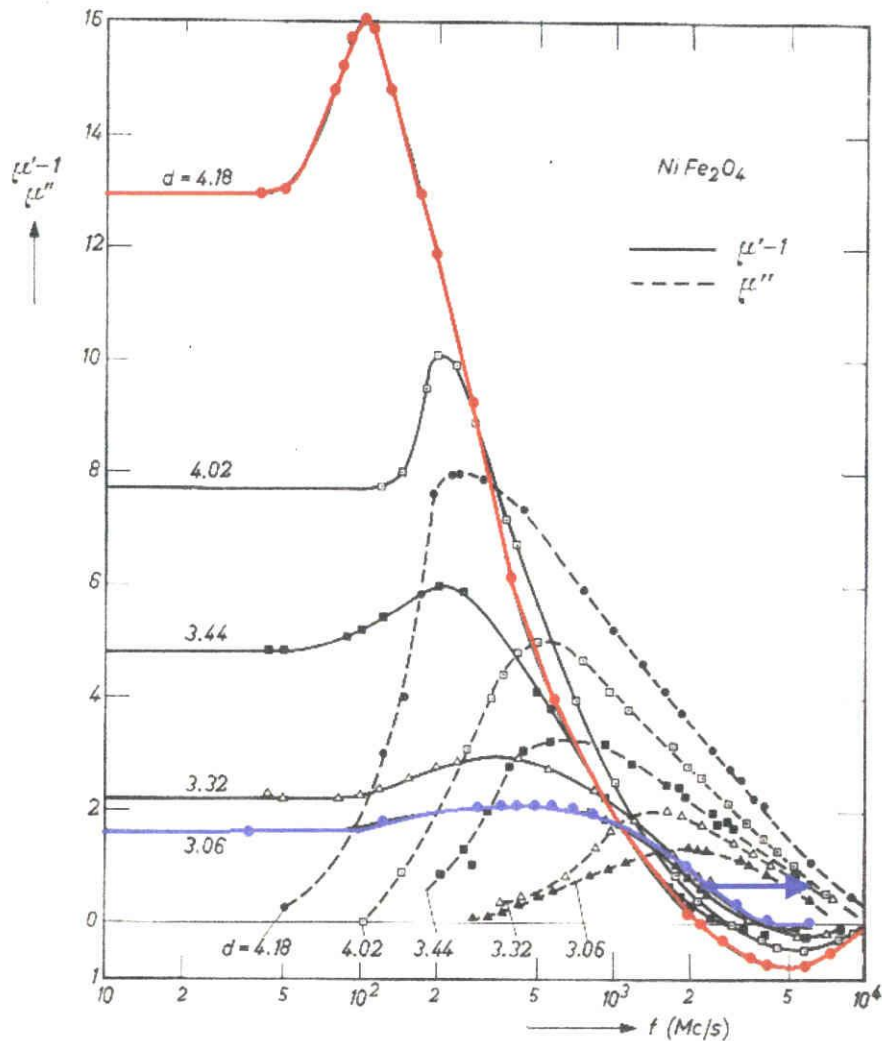
Fig. 50.4. Permeability spectra of incompletely sintered samples of nickel ferrite $NiFe_2O_4$. The five samples were sintered at progressively higher maximum temperatures in the range 960-1327 °C. The densities d of the samples indicated in the figure should be compared with an X-ray density $d_x = 5.38$. After [Br 7].

Figure 1.6 The frequency dependent of Ni-Ferrite related with densities. Adapted from [16]

1.2.5   Magnetic Permeability and applications

The applications of spinel ferrite depend on the shape and the microstructure. For example, Nanosized spinel ferrite particles importance to the microwave industries, high speed digital tape or disk recoding, repulsive suspension for use in levitated

9

railway systems, ferrofluids, catalysis, medical imaging, transformer and magnetic refrigeration systems [17,18, 19]. In the magnetic point of view the ferrite that have magnetoelectric effect are used as sensors, isolators, wave-guides, transducer, electromagnetic/radio frequency interference (EMI/RFI) filter, etc [14].

For EMI filtering/shielding, absorptions contribute to the highest rate of the shielding. The absorptions are effectiveness at certain thickness of the shielding material. The effective thicknesses are also known as skin depth. That means the lower the skin depths are good to have a thinner size of shielding materials needed. The equations below indicates the skin depth δ of the of shielding materials [20];

$$\delta = \frac{1}{\sqrt{\pi f \mu \sigma}}$$

According to the equations, Permeability μ are among the main contributors for reducing the value of the skin depth.

Electromagnetic interference (EMI)- a specific kind of environmental pollution due to a rapid growth in the utilization of electrical and electronic devices in residential, industrial and military applications [57]. The only way to reduce EMI is by shielding [33]. The Ni-Zn ferrites is among the material that widely use for this applications. Recently, the commercialized shielded shape of Ni-Zn ferrite was in single layer and grid shape [36-38]. The ferrite grid has a better performance than single layer ferrite [39] because it has higher and wider frequency absorption bandwidth (figure 1.7). The ferrite grid (figure 1.7) has a large size (mm size).
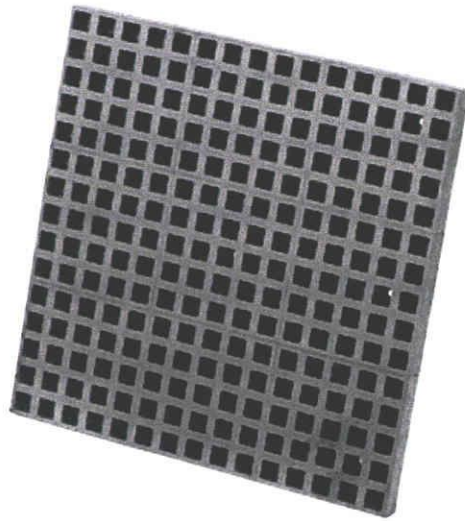
Figure 1.7, the commercialized ferrite grid for EMI shielding applications
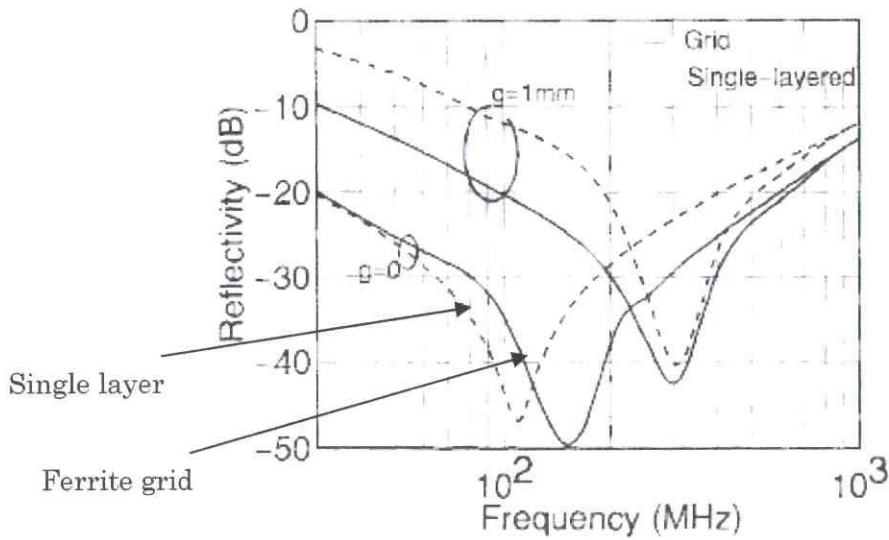
Figure 1.7 Return loss of Single layer and ferrite grid. Adapted from [39]

1.3 Motivations

Discussed in previous sections, it was agreed that for low density ferrite have a lower permeability than that high density. But for lower density ferrite have a better frequency range at higher region before transform from ferrimagnetisms into diamagnetism behavior. Until now the microstructure dependent for the

ferrimagnetism behavior was been widely studied by researchers. The conditions such as physical shape and the grain due to the preparations method were introduced in order to fix the conditions with the application purposes. Currently most of the study had focus at the conditions of film shape [21, 22], Nano-particles (Powder) [17, 18, 23, 24, 25], Bulk [26, 27, 28] etc. Among the famous established condition is film shape and shows the good performance at higher frequency region. According to J. Goa (2004) [21], argue the present bulk ferrite components are employed in discrete devices at microwave frequencies, but they are not compatible with planar circuit design meanwhile the soft ferrite films usable at frequencies higher than several hundred megahertz (MHz) as inductors and wave absorber that required for electric circuit integrations. But for most of the film shape ferrite was produced with non-conventional method, which have the special effect to the magnetic domain. Currently for film shape ferrite, variety of technique had been introduced for preparations of Ni-Zn ferrite. Among the well known method of preparations are [21];

a. Pulsed laser deposition (PLD) [29, 30]

b. Electric beam reactive evaporation

c. Magnetron sputtering

d. Spin-spray ferrite plating

Because of thus reason, this study is focus on the lower density and consist the oriented structure similar to ferrite film that might increase the resonance at higher frequency in order to improve the permeability at GHz frequency region of Spinel ferrite. To produce such ferrite, the appearances of the specimens must in;

1. High porosity conditions

2. Structure consisted layer of wall that similar to ferrite film.

Combinations of thus two factors might improve the permeability at the higher frequency regions. Therefore ceramizations of woods by conventional sintering methods was introduced in this study. We have found that the wood is a good candidate because it contained of elongated tubular cells aligned with the axis of the tree trunk [1]. Cedar type was choose due to the pores that almost uniform sizes. In additions of that, recently the ferrite grid has a better performance than single layer ferrite. Meanwhile, physically ferrite wood have a similar shape as ferrite grid, but ferrite wood have a micro sizes.

Some researcher had study related with wood and Iron oxide. Zhaoting Liu et al (2005) [2] was prepared iron oxide from wood template. In the study was only focus on the preparations of Fe_2O_3 with trigonal-hezagonal scalenohedral crystral structure (Non-spinel) and no magnetic study was conducted.

Meanwhile K.H.Wu et al (2006) have prepared the charcoal NiZn ferrite. The specimens were prepared at low temperature and the wood component retained as composite (not complete single phase NiZn ferrite). Only the FMR results were shown in this study.

Hideo Oka et al (1999) – (2004)[61 – 64] have study about magnetic wood that implemented at indoor furniture. The complete magnetic study was conducted. But the wood honeycomb microstructure doesn't exist in the specimens. The magnetic wood are;

1. Powder coated onto a fiber board
2. Powder and wood powder mixed and pressed into board (no wood microstructure)
3. Wood impregnated with water based magnetic fluid
4. Combination structure consisting of a fibre board layer/ magnetic

binder layer/ fibre board layer

1.4   Thesis statement and thesis organization Main Objective

The aims of this study are to develop the mixed spinel ferrites (Ni-Zn ferrite and Mn-Zn ferrite) and Ba-ferrite by using wood templates that might improve the permeability at the higher frequency regions. This thesis is contribute to the new condition of microstructures that consisted the systematic array of the pores that mimicking wood templates. In the other hand, due to the condition of thus microstructure was contributing to the new phenomena of magnetic properties that similar tendency with film shape. These low density ferrite woods have microstructures that contribute to the main roll at higher frequency. Finally to determined the Return loss of thus ferrite wood in the higher frequency regions for the selected ferrite woods

In Chapter 2, this chapter is stress on the experiment procedure that include; the determination of crystallizations of single phase ferrite by controlling the sintering temperatures, times and atmosphere. Thus preparation methods were decided due to the review of the previous study. Beside that, the methods of physical characterizations of ferrite were suggested. The second parts of this chapter were described about the method of magnetic measurements. Currently, most of the equipment was used to measure the powder and film shape ferrite. The technique to determine the effect by the woody microstructure was introduced too. The approached to determine the magnetic effect and the Return loss of woody microstructure was stated.

In Chapter 3, the optimum preparation conditions of ferrite wood were presented. The transformations mechanisms were also determined by using combination of appropriate equipment such as DT-TGA and XRD analysis. The different preparation conditions were revealed between thus soft ferrites. As a results thus ferrite wood was

successfully prepared with a minimum defects. The characterizations of thus ferrite wood were also mentioned.

Chapter 4, Magnetic hysteresis (B-H curve) of ferrite wood in cubical shape was investigated. Normally for soft ferrite, in bulk conditions the hysteresis is isotropic in any direction that measured with the same thickness. But for ferrite wood even tough the physical appearances look like bulk ferrite, but the magnetic hysteresis anisotropy was revealed (easy axis and hard axis). This phenomenon similar with the film shape ferrite because ferrite wood are reacting like multilayered ferrite film. The final results was concluded the contribution of the ferrite wood at the higher frequency regions. The Return loss of the ferrite wood was presented.

Finally in Chapter 5, the remarkable finding in this study was concluded. The present works are stated and the recommendations of future development are stated.

CHAPTER 2

EXPERIMENTAL PROCEDURE

2.1   Introduction

This chapter discussed about the experimental procedure and the methods were used in order to preparation and characterization of mixed spinel ferrite wood.

The method and the used equipment of examined the desired properties were stated. The microstructures were visually confirmed by using Scanning Electron Microscopy, SEM. The compositions of the products were validated via X-Ray diffraction (Cu-Kα). In the next part of this study was involving the magnetic properties of the ferrite wood. Beside that the properties of ferrite wood was determined. Among the characteristic that involved are, Crystallographic, Physical and ferrimagnetic behavior.

The focus of this study are prepared and characterization of ferrite wood. Two main points were considered, which are

1.   Preparations

-        Characterizations

2.   Magnetic behavior

-        Magnetic hysteresis curve

-        Magnetic permeability

The optimum preparations methods are necessary before the characterizations. The preparation method involved the evaluations of the physical structure that affected by the wood template, sintered conditions/temperature/time, phase confirmations and etc.

After the optimum preparations method obtained, the study was continuing by

characterization of ferrite wood. The following experiments were conducted for the characterization of ferrite wood.

1. Structural analysis

  - Lattice parameter determinations

  - Bulk density and theoretical density

  - Porosity

  - Shrinkages

  - Microstructure

2. Magnetic properties

2.2 Preparation of ferrite wood.

Preparation of Ni-Zn Fe_2O_4 and Mn-Zn Fe_2O_4 from wood template requires composition validation and retaining the microstructure of templates. The wood template was originally containing the organic composition such as gums, troplones, fats and fatty acids [2], and mostly Carbon. The preparation Ni-Zn ferrite and Mn-Zn ferrite that mimicking the wood templates is among the main objectives of this study. In order to produce such ferrite wood, the external appearance and the composition validation is necessary. After preparing the ferrite wood, the magnetic properties of ferrite wood affected by thus microstructure is investigated. Spinel mixed ferrites that mimicking the wood template are prepared. Figure 2.1 shows the preparations process of ferrite wood. The precursor

Meanwhile in order to hexagonal ferrite that mimicking wood template the preparations of precursor solution was slightly different with spinel ferrite due to the solubility of $Ba(NO_3)_2$. $Ba(NO_3)_2$ are only solute with certain temperature and PH and ethylene glycol as solvent. Jianxun Qiu et al [53] was prepared the precursor material by

dissolved the of $Ba(NO_3)_2$ and $Fe(NO_3)_3$ into deionized water by the addition of citric acid. Meanwhile Wen-Tsang Liu et al [54] was use ethylene glycol as the solvent. Figure 2.2 explained the preparations method of the precursor solutions for preparations of $BaFe_{12}O_{19}$ wood.

Preparation of Ni-Zn ferrite and Mn-Zn ferrite mimicking wood template	
Template preparation	Precursor solution preparation

Infiltrations
Sintering
(Ni-Zn ferrite and Mn-Zn ferrite) **Ferrite wood**
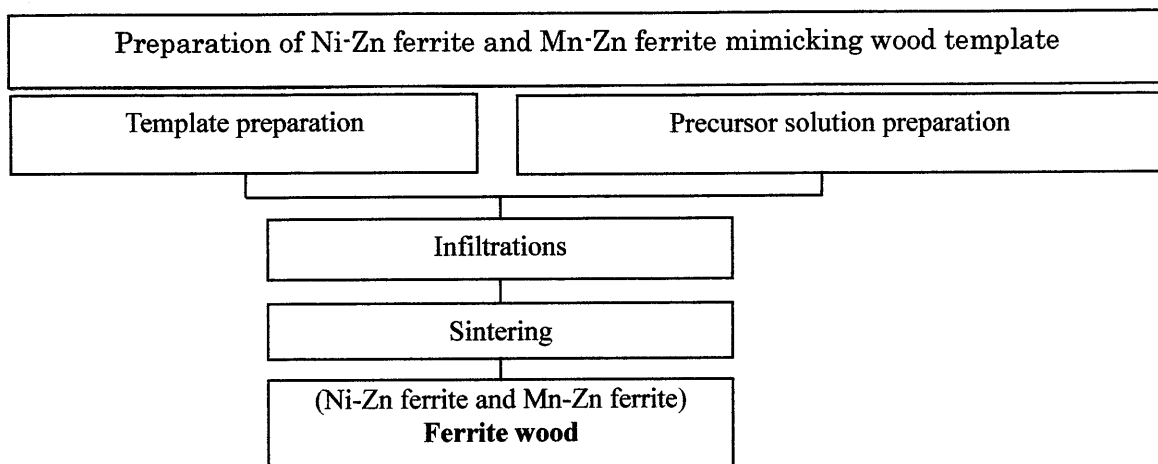
Fig 2.1 Preparation process of MnZn-ferrite and NiZn-ferrite wood

$Ba(NO_3)_2$	$Fe(NO_3)_3.9H_2O$

Citric Acid	

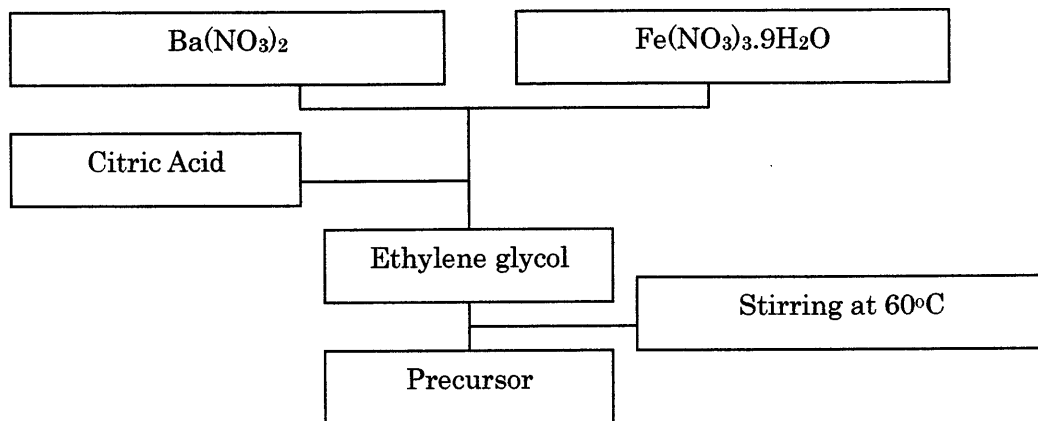| Ethylene glycol	
	Stirring at 60°C
Precursor	

Fig 2.2 Preparation of precursor solutions for Ba-Ferrite wood

2.2.1 Template preparation

Wood was prepared as a template. The wood had been treated before the next processes in order to increase the effective absorption of sol. The wood template was originally containing the organic composition such as gums, troplones, fats and fatty acids [2],

18

and mostly Carbon. Initially the thus organics were mostly water proof and influencing the effectiveness of absorption of precursor solution.

The wood template was treated by boiling with water and 25% ammonia for 1 h to remove the wood extracting compounds. The wood templates were washed with distilled water before they were re-boiled with de-ionized water for 1-2 h. Figure 2.3 shows the both treated and untreated template with water drop. It obviously shows the treated template have a better absorption compared to untreated template.
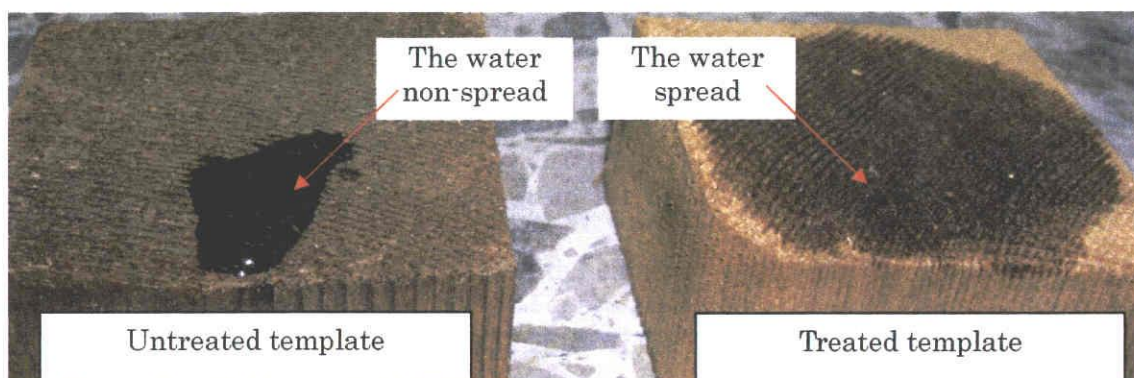
Figure 2.3 Untreated and treated template with water drop

After the wood template treated, the connectivity among the pores was improved.

2.2.2   Preparation of precursor solution

The commercially available $Ni(NO_3)_2.6H_2O$ (Ni(II) Nitrate hexahydrate) Wako, $Fe(NO_3)_3.9H_2O$ (Iron(III) Nitrate Enneahydrate) Wako, $Zn(NO_3)_2.H_2O$ (Zinc Nitrate Hexahydrate) Wako and $Mn(NO_3)_2.6H_2O$ (Manganese (II) Nitrate Hexahydrate) wako, was used for the precursor solution. Thus Nitrate was weighted according to the required stoichiometric proportion (1 Molar). The compositions were mixed with de-ionized water and stirred constantly until all the solute dissolved.

Table 2.1, 2.2 and 2.3 indicates the amount of the compositions of Nitrate precursor solution for 1 Molar/litre stoichiometirc proportions for $Ni_xZn_{1-x}Fe_2O_4$, $Mn_xZn_{1-x}Fe_2O_4$ and

$BaFe_{12}O_{19}$. The total prepared of thus precursor solution is 200ml.

Table 2.1 Amount of Nickel nitrate, Zinc nitrate and Iron Nitrate for precursor solution

(200ml) to prepared Ni_xZn_{1-x} ferrite (x = 0.1, 0.5 and 0.9)

Element	Weight/ mol (L)	Ratio,(x)	Weight, (g)
$Ni(NO_3)_3$	290.79	0.1	1.939
		0.5	9.693
		0.9	17.447
$Zn(NO_3)_3$	297.49	0.1	17.849
		0.5	9.916
		0.9	1.983
$Fe(NO_3)_3$	404.00	0.1, 0.5 & 0.9	53.867

Table 2.2 Amount of Manganese nitrate, Zinc nitrate and Iron Nitrate for precursor solution

(200ml) to prepared Mn_xZn_{1-x} ferrite (x = 0.1, 0.5 and 0.9)

Element	Weight/ mol (L)	Ratio,(x)	Weight, (g)
$Mn(NO_3)_2$	290.79	0.1	1.913
		0.5	9.568
		0.9	17.222
$Zn(NO_3)_3$	297.49	0.1	17.849
		0.5	9.916
		0.9	1.983
$Fe(NO_3)_3$	404.00	0.1, 0.5 & 0.9	53.867

Table 2.3 Amount of Barium nitrate, Citric acid and Iron Nitrate for precursor solution

(200ml) to prepared $BaFe_{12}O_{19}$.

Element	Weight/mol (L)	Ratio,(x)	Weight, (g)
Ba(NO3)2	261.336		4.02
Fe(NO3)3	404.00		74.59
Citric acid	192		57.6

2.2.3   Infiltrations

Infiltration process is a mechanism for the precursor solutions absorbed inside the body of the template. Some study used the capillary action for the infiltration process. But capillary action must infiltrate perpendicular to the fluid surface. For capillary action it must have an open capillary (pores) that allowed the air escape (flow out to atmosphere). If the pores are covered with dust or dirt, the air will trap inside the template and caused the capillary action failure. The capillary action method also limited to the certain height that explained by equations [1] below.

$$h_{max} = 4\gamma cos\varphi/(d_{co}\rho 1g)$$

where;

ρ= density of precursor, φ= wetting angle, γ= surface tensions, d_{co}= diameter of pores

In this study, the natural flow from high concentrations to low until archiving equilibrium state was applied for the better infiltrations. Osmosis process were involved which is the body of wood was react as membrane wall.   The treated specimens (section 2.21) with boiling the template for few hours. In the other purpose this process also release the air inside the template and the water that have lower viscosity absorb inside the pores and

the body of the template. After that the wet template immediately deep inside the precursor solution and keep fully immerge. The natural mixing was occurred in this process which is the water and the precursor will flow until achieving the equilibrium state. Followed by the osmosis process which is the precursor solution absorb inside the body of the template. In the higher temperature will have a faster time to achieve the equilibrium state due to the kinetic energy of the liquid that move faster but in higher will caused the evaporation of the liquid.
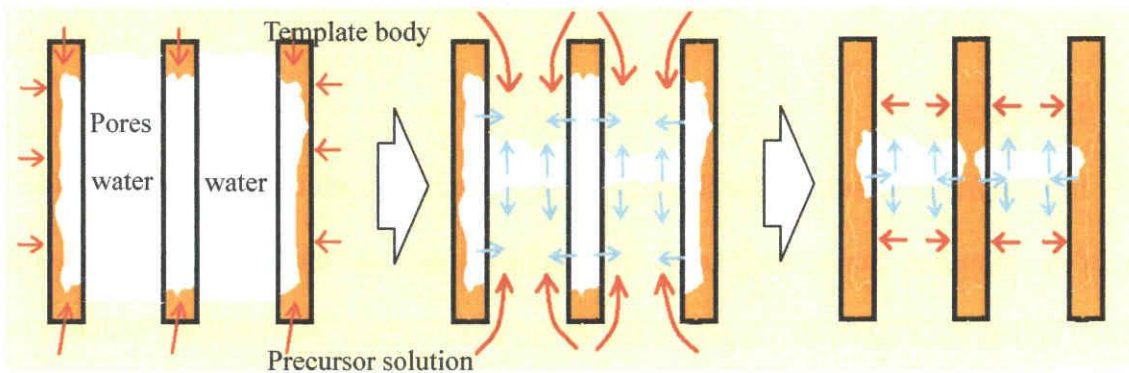
Figure 2.4 Infiltration process

Figure 2.4 shows the infiltration mechanism of the precursor solutions inside the template. The precursor was absorbed by the template outside wall and flow inside the pores and absorbed by the internal wall of template. For this process, the templates were keep fully immerge into the precursor solution for 6 – 7 days.

To determine the complete infiltration, it was examined by slicing the middle of the template, which is show in figure 2.5. The infiltrated wood templates have a darker color.
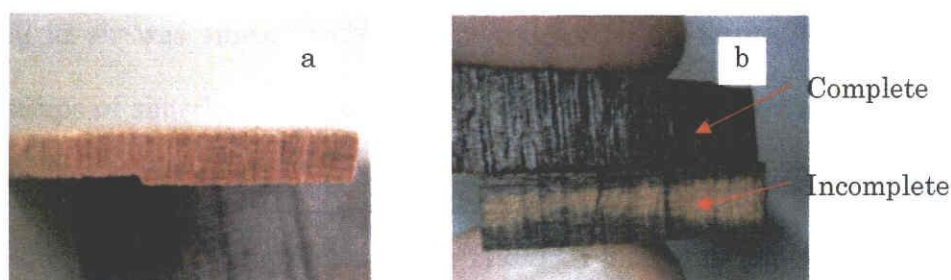
Figure 2.5. Images of the (a) Template before infiltration, (b) Templates with complete and incomplete infiltrations.

The color of the cross section of template indicates the complete or incomplete infiltration, which is for darker region indicate the portion penetrated by the (nickel nitrate + zinc nitrate + Iron (III) nitrate or manganese nitrate + zinc nitrate + Iron (III) nitrate) precursor solutions. To attempt the good output the complete infiltration is necessary.

2.2.4   Sintering

2.2.4.1   Sintering of Ni-Zn ferrite

The infiltrated template was sintered at various temperatures to determine the most optimum temperature and sintering time. For each sets of attempt, the initial temperature was set by rising for 6h to reach the target temperature (figure 2.6). Most of the study reported for preparing the Ni-Zn ferrite the template was sintered in air [21] because the Oxygen is needed for the necessary reactions. S.Deka [17] was prepared the $Ni_{0.5}Zn_{0.5}Fe_2O_4$ with Iron nitrate, Zinc Nitrate and Nickel Nitrate and calcine in air with the temperature range 200-1000°C. He also prepared by Fe_2O_3, ZnO and NiO at 1100°C in air. Meanwhile A.Verma et al [26] was sintered 1000°C for 1 h in order to prepare Ni-Zn ferrite from the Nickel nitrate, Zinc Nitrate ad Iron III citrate. As a conclusion, preparing the Ni-Zn ferrite via conventional method must in air at the temperature more than 1000°C (possibly for oxidation reactions). Finally the temperature was reduced to room temperature R_t within 6h.
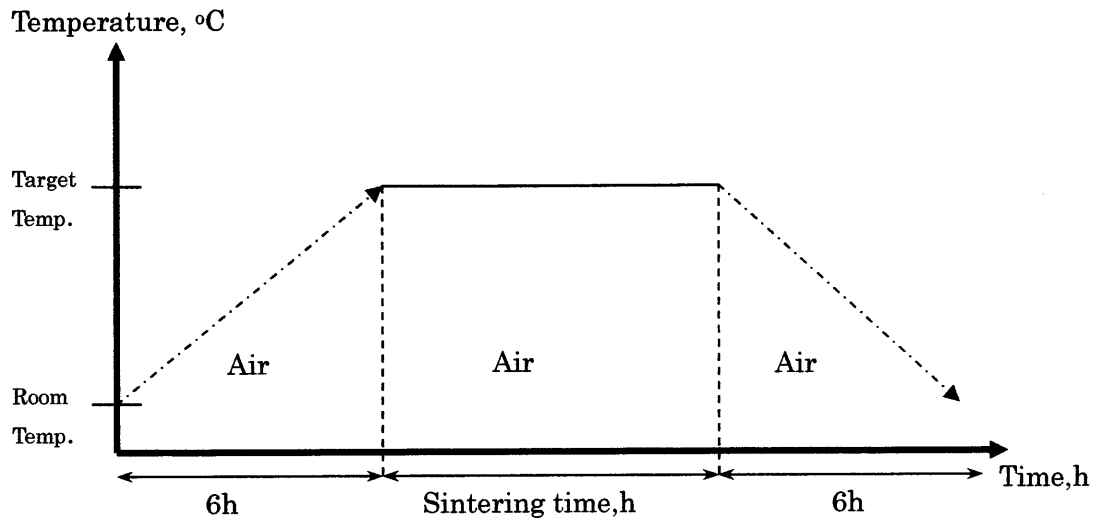
Temperature, °C

Target
Temp.

Room
Temp.

Air

Air

Air

6h   Sintering time,h   6h   Time,h

Figure 2.6 Temperature vs sintering time for Ni-Zn ferrite

2.2.4.2 Sintering of Mn-Zn ferrite

Even tough Ni-Zn ferrite and Mn-Zn ferrite have a similar spinel structures but the sintering methods might be different. Jae-Gwang Lee et al. (2006) was prepared the Mn-Zn ferrite powder using conventional method by annealed at 800°C for 4h and followed by second annealing at 1300°C for 12h in vacuum. S.M.Attia (2006) have a different opinion, he also have prepared via mixed oxide by ground for 4 h by an electrical grinding machine and the mixtures were pre-sintered at 900°C in air. Pre-sintered specimens were shaped into desire shape and sintered at 1200°C for 5h in air. The reason some of the study suggest the sintering conditions of Mn-Zn ferrite must in free air conditions, because according [31], slowly cooled in N_2 atmosphere is necessary to prevent segregation of α-Fe_2O_4. The review was found that, the sintering conditions of Mn-Zn ferrite was sintered in air and some are non-air. Because of that reason this study was attempt in both conditions. For this study, the Mn-Zn ferrite was sintered in,

1.   Air

2.   Argon atmosphere.

Sintering in air was similar with the sintering or Ni-Zn ferrite (section 2.2.4.1). Meanwhile the setups of sintering in argon are show in figure. The ceramic tube was located in the furnace (figure 2.7). At the early stage, the specimens were sintered in air to remove the wood organic. After reach the target temperature (1200°C) the argon gas was flow in one direction at 5 ml/s (figure 2.8).

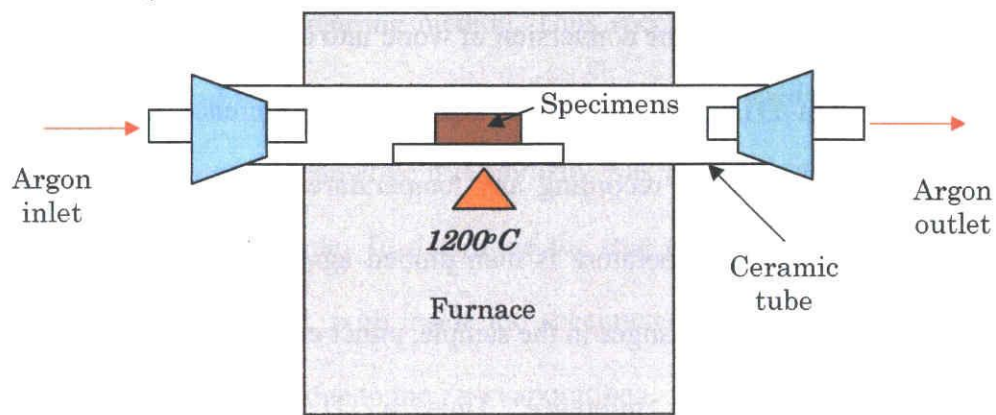Figure 2.7; Sintering of Mn-Zn ferrite in argon atmosphere.

The argon atmosphere was retained until the cooling process complete. The free air (especially oxygen) environment was expected inside the tube during the sintered period due to the flowed argon gas. Argon gas was chosen because it chemically stable characteristic.
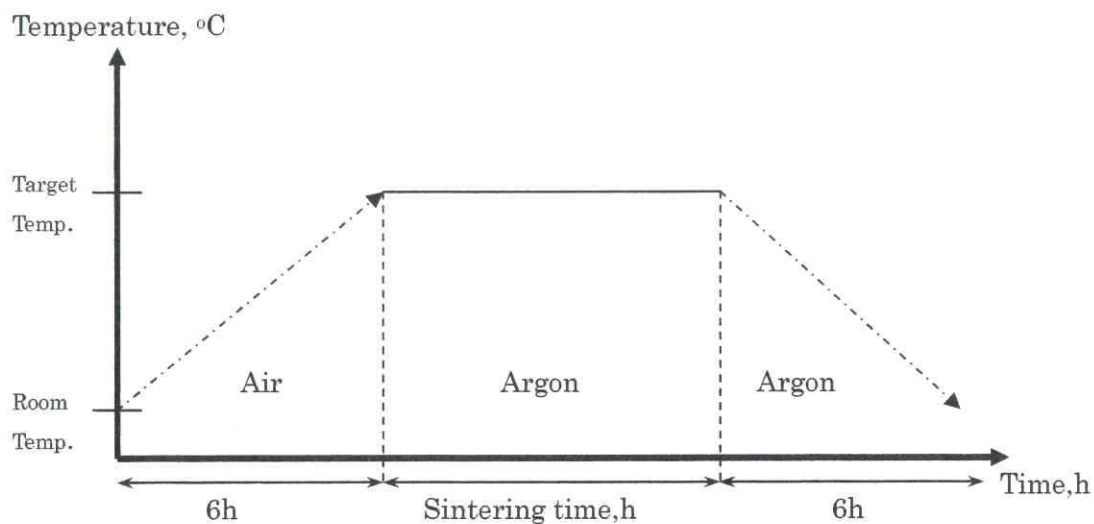

Figure 2.8 Temperature vs sintering time for Mn-Zn ferrite in argon atmosphere

2.3   Diffrential Thermal Analysis DTA , Thermogravimetric analysis TGA

The DTA-TG was conducted by using simultaneous DTA-TG apparatus (DTG –

60H Shimadzu). This thermal analysis was performed in air at heating rate of $10^{\circ}C$ / min from

room temperature to $1200^{\circ}C$. The standard reference specimen was Al_2O_3.

These measurement settings are similar with the study conducted by D. Mallick

(2007)[6] that also investigates the conversion of wood into ceramics. But for this study it was

conducted in air.   In DTA, the specimens and an inert reference are made to perform

identical thermal cycles, while recording any temperature difference between sample and

reference. This differential temperature is then plotted against time, or against temperature

(DTA curve or thermogram). Changes in the sample, either exothermic or endothermic, can be

detected relative to the inert reference. Thus, a DTA curve provides data on the

transformations that have occurred, such as glass transitions, crystallization, melting and

sublimation. The area under a DTA peak is the enthalpy change and is not affected by the heat

capacity of the sample.

For the infiltrated woods specimen, the peak exothermic or endothermic might be

caused by either wood itself or the infiltrated material. To ensure such different, the different

conditions of specimens were examined such as;

1.   Infiltrated wood

2.   Wood only

3.   Dry Infiltrated precursor

TGA is a type of testing that is performed on samples to determine changes in

weight in relation to change in temperature. Such analysis relies on a high degree of precision

in three measurements: weight, temperature, and temperature change. As many weight loss

curves look similar, the weight loss curve may require transformation before results may be

interpreted. A derivative weight loss curve can be used to tell the point at which weight loss is most apparent and remaining weight.

2.4   Porosity and Density measurement of Ferrite Wood

Bulk density is related with the porosity of material. J. Bera at al. (2005)[32] were used archenemies principle to determined the bulk density and porosities of $Ni_{0.7}Zn_{0.3}Fe_2O_4$ that prepared via conventional sintering method. Thus specimens consist 2 type of porosity namely, open porosity and true porosity. Open porosity only examined the pores that exist in the surface of the specimens. Meanwhile true porosity was involved internal pores that can't measure via archenemies principle. To determine the true porosity, the X- ray density was involved.   They also stated that, pore inside the specimens' prepared conventional sintered Ni-Zn ferrite difficult to remove due to the Zn evaporations.

2.4.1   Theoretical Density

Technically ferrite wood consists the 1 directional connected pores that exposed at the surface. That means the open porosity = true porosity. Meanwhile the theoretical density of ferrite wood can be calculated via lattice constant obtain from XRD measurement formula below

$$d_x = 8M/(Na^3)$$

Where, M is the molecular weight, N is the Avogadro's number and a is the lattice constant derived from XRD data [33].

2.4.2   Bulk Density (Experimental)

Bulk density of ferrite wood was measured by AG 206 Mettler Toledo density kit (figure 2.9).

Figure 2.9 AG 206 Mettler Toledo density kit via archenemies principle

Because of very small pores size, the ferrite woods are difficult to direct examined by this equipment (the air difficult to escape when deep inside the water). The procedure determines the bulk density is stated as below.

1. Slice the surfaces of the specimens, for the pores exposure

2. Measured the ferrite wood weight, W_f

3. Ferrite wood drop with low viscosity polymers binder to cover the pores. The polymer binder must fully flow inside the pores (no air trap)

4. The dried ferrite wood with polymer binder was measure the weight, W_{fb}.

5. percentage contain of ferrite wood was determine

$$\% \ W_f = W_f / \ W_{fb}$$

5. Measure the density, ρ_c of the specimens by AG 206 Mettler Toledo density kit.   The concept measurement of the equipment used archenemies principle.

6. Calculate the volume, V_c of non homogeneous shape of ferrite wood

$$V_c = W_{fb} / \rho_c$$

7. The bulk density of ferrite wood was determined by

$$\rho_f = W_f / V_c = (\% W_f \text{ x } W_{fb}) / (W_{fb} / \rho_c)$$

● Small error might occur due to remained air and overflowed binder (figure 2.10).
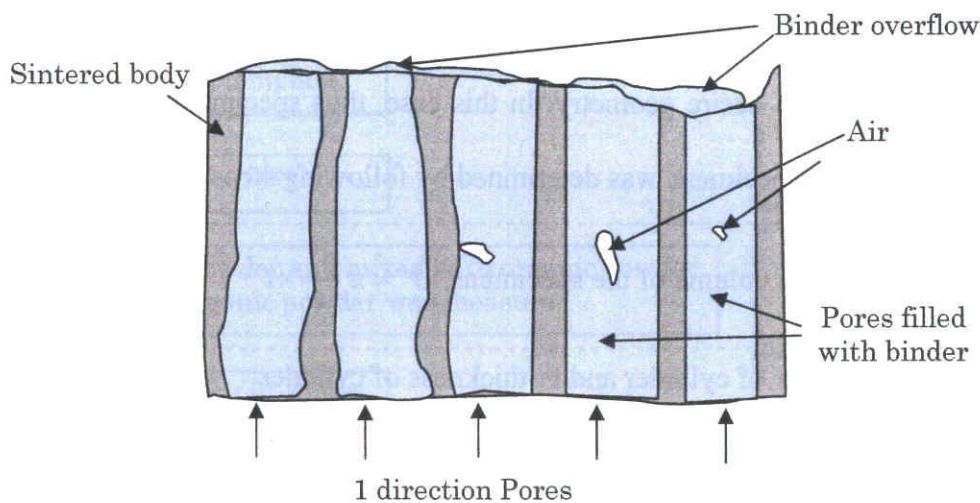
1 direction Pores
Figure 2.10; schematic of ferrite wood filled with polymer binder

2.4.3   Density calculations via SEM images

.The overall area measured = **sintered body + pores (air) = πD_{avg}^2**

The area occupied by sintered body = **Thickness x circumference = πD_{mean} x t**

$$D_{mean} = D_{avg} - (t/2)$$

Theoretical density of $Ni_{0.5}Zn_{0.5}Fe_2O_4$ = **5.31 g/cc**

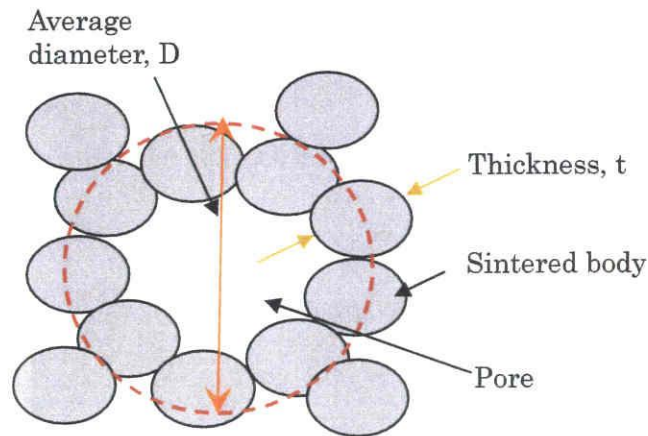Bulk density = **$(\pi D \text{ x } t)/(\pi D^2) \text{ x } 5.31 g/cc$**

Figure 2.11; The parameter of 1 unit cell for bulk density calculation

2.4.4 Density of non- wood ferrite

The high porosity of non-wood ferrite was conducted in different approach. Since the internal pores are un-expose, it can't be measured via Archenemies principle. But non-wood ferrite was easy to shape into desire geometry. In this case, thus specimens were shape into cylinder. The density of the specimens was determined by following steps;

1. Measure the volume of the specimens, $V = \pi \dfrac{d^2}{4} \times t$

    d = diameter of cylinder and t= thickness of cylinder

2. Measure the weight of the specimens, W

The bulk densities, ρ for non- wood ferrite are $\rho = \dfrac{W}{\pi \dfrac{d^2}{4} \times t}$ (g/cm^3)

2.5 Preparations of Non-Wood shape ferrite

The non-wood shape ferrite was prepared for the comparison with ferrite wood. For the better comparison purpose the non-wood shape ferrite must have;

1. Similar compositions

2. Similar grain

3.   Comparable porosity/density

4.   Non-wood microstructure

To get the similar compositions with ferrite wood, the non-wood shape ferrite was prepared from same material. The non- wood shape ferrite was prepared by the calcined wood template and crushed into powder and compressed into cylinder shape. So in this case it has the exactly same material base. To control the porosity / density, the specimens were mixed with organic powder and sinter. Stated below are the procedures to produce such specimens (figure 2.12);
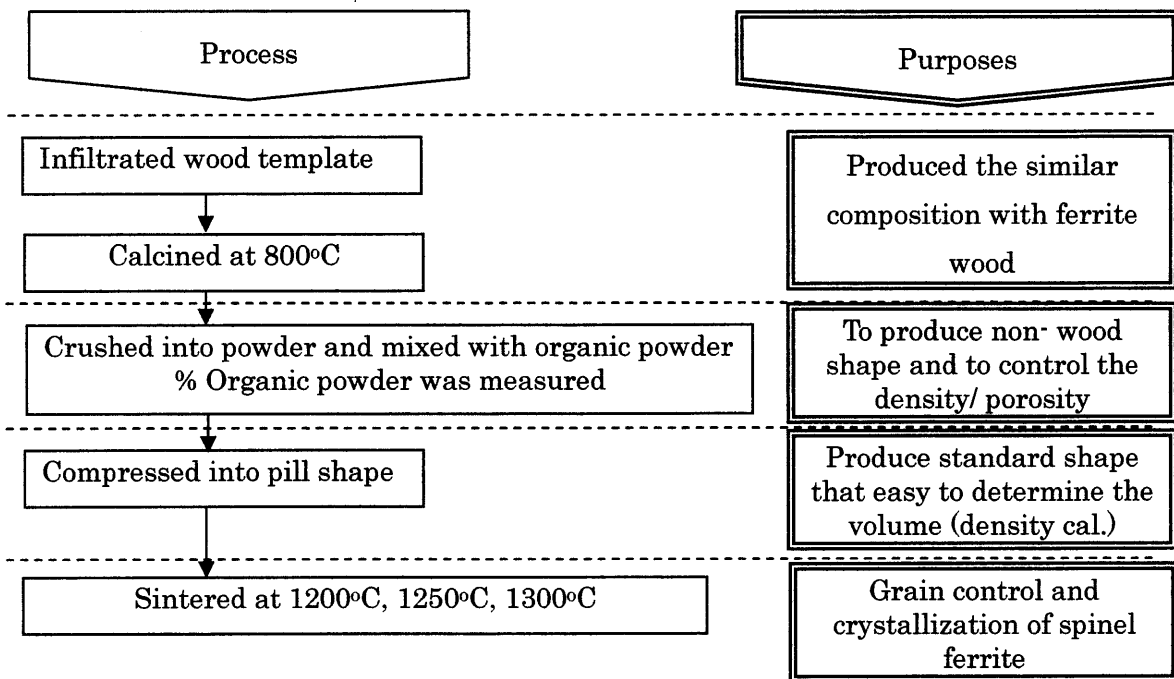
Process	Purposes
Infiltrated wood template	Produced the similar composition with ferrite wood
Calcined at 800°C	
Crushed into powder and mixed with organic powder % Organic powder was measured	To produce non- wood shape and to control the density/ porosity
Compressed into pill shape	Produce standard shape that easy to determine the volume (density cal.)
Sintered at 1200°C, 1250°C, 1300°C	Grain control and crystallization of spinel ferrite

Figure 2.12 Preparation method of Non-wood shape ferrite

2.6   Scanning Electron Microscopy, SEM

The microstructures of the specimens were examined by Scanning Electron Microscopy, SEM (JSM-6100 JOEL). The specimens were cut into small shape that fit into sample holder. Carbon paste were used for bind the specimens with the holder and dried for 2

h into dryer.

To confirm the microstructure of wood retained, the specimens were examined in 2 different directions (figure 2.13). At the surface, the pores might be covered up. It was suggested to slice the specimens for the better visual examinations.
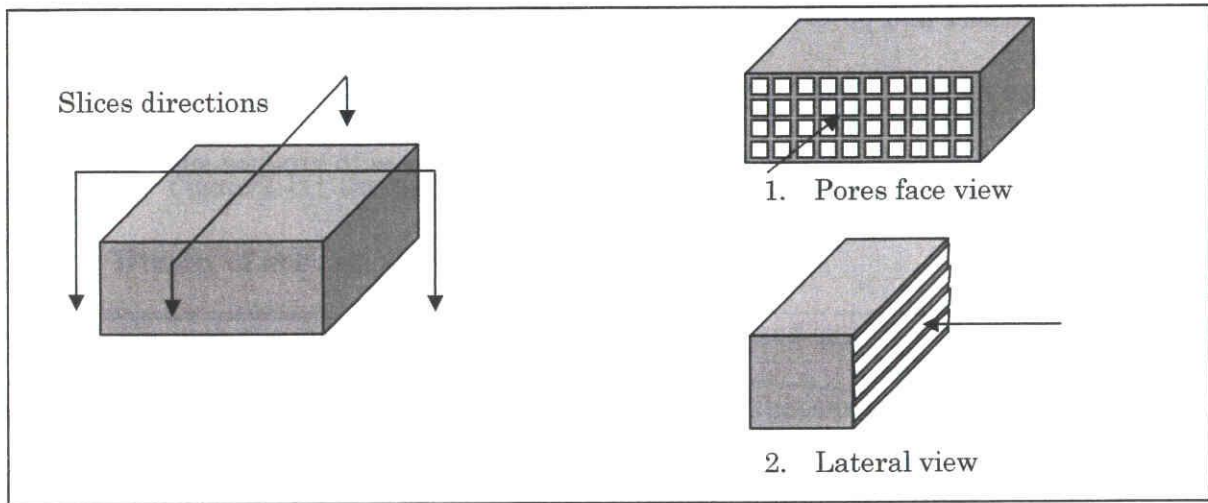

Figure 2.13 The expected face of the ferrite wood for SEM

2.7 Lattice of ferrite wood

The crystal structures of the specimens were investigated with XRD (RINT 1100, Rigaku) with Cu-Kα radiations. The radiations angle was at $0.02°$ for every point from $2\theta = 20°$ to $80°$. The angle was selected because the entire main peaks for spinel ferrite are within the range. S. Deka and P.A Joy was examined Ni-Zn ferrite with Cu-Kα radiations at the angle of $2\theta =$ from $10°$ to $80°$. They were found that only a small peak (111) revealed at below $20°$.

From the XRD pattern the lattice parameter were determined by the basic *Bragg's* equations.

$$\lambda = 2d \sin \theta$$

Which wavelength of incident wave, λ of Cu-Kα are 1.5405 meanwhile for this spinel were form by a cubical structural and can be expressed as

$$d_{hkl} = \frac{a}{\sqrt{h^2 + k^2 + l^2}}$$

Which is $(h\ k\ l)$ referred to the crystallographic planes and "a" represent the lattice constant.

2.8   Magnetic Properties

2.8.1   Hysteresis curve

If an alternating field is applied to soft magnetic material, the hysteresis curve is obtained. Figure 2.14 shows the concept of the magnetizations. For high field strengths the attainable flux density is reached. This is known as saturation of magnetization Ms.
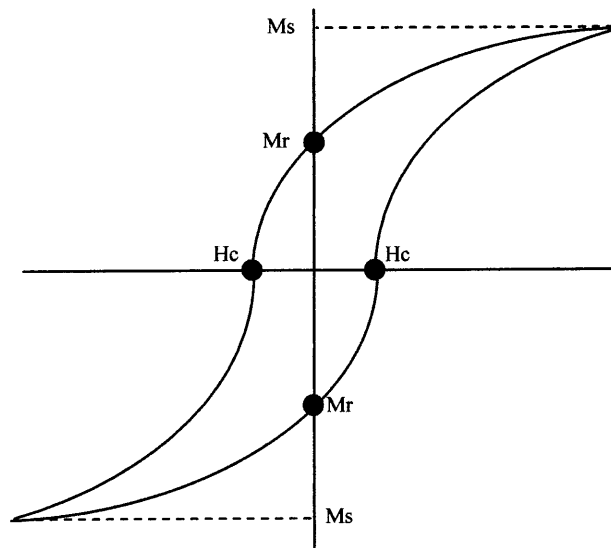
Figure 2.14 Typical hysteresis loop of soft ferrite

If the field is removed, the material returns to the state where a certain magnetization remains. This is the remanent of magnetization Mr. The remanent return to zero for certain negative strength which is referred as coercivity, Hc. As with any hysteretic process, the area inside the magnetization curve during one cycle is work that is performed on the magnet. Common dissipative processes in magnetic materials include magnetostriction and domain wall motion. The coercivity is a measure of the degree of magnetic hysteresis and therefore characterizes the lossiness of soft magnetic materials for their common applications.

2.9   Magnetic hysteresis measurement

The vibrating-sample magnetometer (VSM) is identical in principle to the vibrating-coil magnetometer except that the sample is moved instead of the coil. A VSM is really a gradiometer measuring the difference in magnetic induction between a region of space with and without the specimen. It therefore gives a direct measure of the magnetization. The specimen in general has to be rather short to fit between poles of the electromagnet. The method is therefore in most cases not well suited to the determination of the magnetization curve or hysteresis loop because of the demagnetizing effects associated with the short specimen.

The film shape Ni-Zn ferrite shows the great magnetic properties which are the anisotropy of coercive force increase by increasing of contain of Ni [1] due to the hysteresis anisotropy.

2.9.1   VSM Specimens setup

As illustrate in Figure 2.14(a) the specimen was cut into cubic shape (height ≈ width ≈ length). A and C are perpendicular to the thin layer wall and B is parallel. Magnetic hystereses of the cubic-shaped specimens were measured in the A, B and C directions by VSM as shown in Fig 2.15 (b).

The cubical shape specimens were used in for magnetic hysteresis measured by VSM because for reduce or eliminated the error due diamagnetic effect.
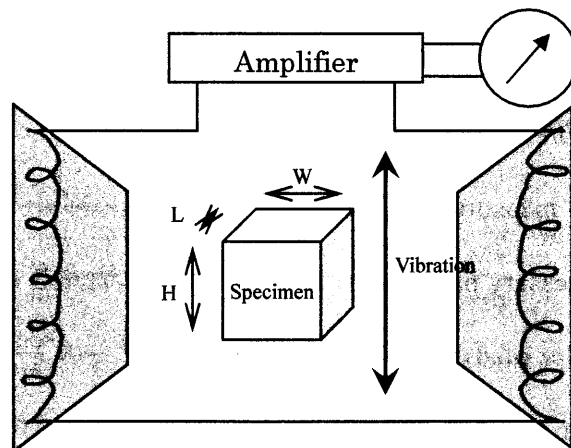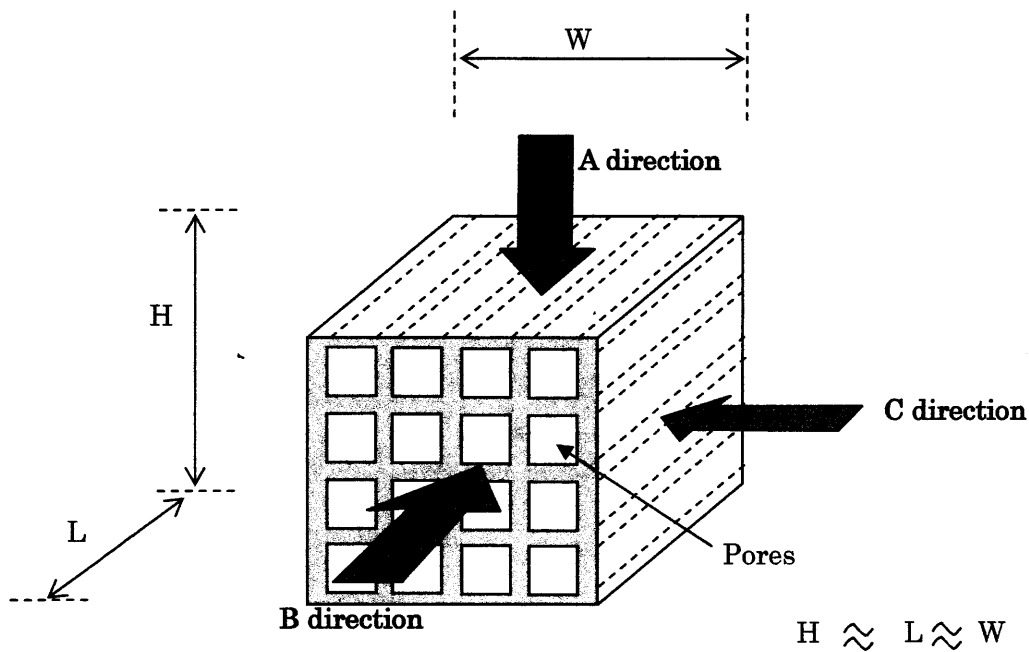
Figure 2.15 Specimens setup for VSM Measurements

2.10 Magnetic permeability

Magnetic permeability is the measure of the ability of a material to support the formation of a magnetic field within itself. In order to dealing with high frequency magnetic field, the complex permeability is a useful tool. The complex permeability can be explained by equation below.

$$\mu(f) = \mu'(f) - j\mu''(f)$$

Which is μ = complex permeability, μ' = real permeability and μ''= imaginary permeability.

In the other word, the μ is a resultant of μ' and μ''
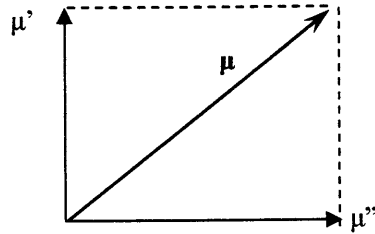
and solving for μ

$$\mu = \sqrt{((\mu')^2 + (\mu'')^2)}$$

In permeability also can be determined from the magnetic hysteresis that measured by magnetization, B vs coercive force, H.

$$\mu = B/H$$

The permeability was measured by. The sizes of specimens are limited to 1 x 5x 6 mm^3. This equipment need necessary parameter obtained from hysteresis curve.

2.10.1   Magnetic Permeability measurements

According to J.Gao et al. (2004)[21] for the non-film $Ni_xZn_{1-x}Fe_2O_4$ have a highest magnetization saturation when x = 0.5. Because of that reason $Ni_{0.5}Zn_{0.5}Fe_2O_4$ woods were chosen for the magnetic permeability measurement. To measure the magnetic permeability of ferrite wood, 1 mm thickness and 6 mm width specimens are required. At first the magnetic hysteresis of ferrite wood were measured to obtain the desired parameter, Ms (Gauss) and Hk (Oe). The ferrite woods were measured in 2 directions.

The magnetic permeability of ferrite wood was measured by Agilent E 5070B ENA series Network analyzer attach with Ryowa PMF-300. The maximum thicknesses of the specimens for the measurement are 1mm and the widths and length are 6mm (figure 2.16).
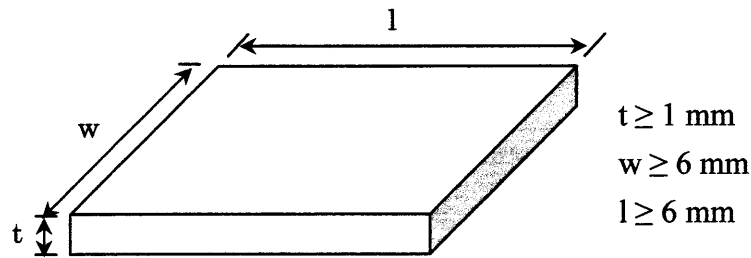
t ≥ 1 mm
w ≥ 6 mm
l ≥ 6 mm

Figure 2.16 Specimens sizes for Magnetic permeability measurements

The principle measurements of the equipment are shown in figure 2.17. The direct currents have been applied in 1 turn coil and generated 1 direction DC magnetic field. The easy axis was in parallel with the coil.

The relative permeability was obtained by (equations) determined the Impedance when a sample is saturated Z_{ino}, Impedance when a sample is unsaturated Z_{ins}, Output voltage when a sample is unsaturated V_s and Output voltages when a sample is saturated V_o.

$$\mu_r = [S_c/(d_m \times t_m) \times \{((Z_{ins} + 50) \times V_s)/((Z_{ino} + 50) \times V_o) -1\}] + 1$$

which is μ_r = relative permeability

t_m = Sample thickness

S_c = Cross Section area of sensor coil

d_m = Sample width

DC Magnetic Field

I Drive Coil

Gain
Phase
Impedance

Sample Inside   Shielded Loop Coil

RF Mag. Field

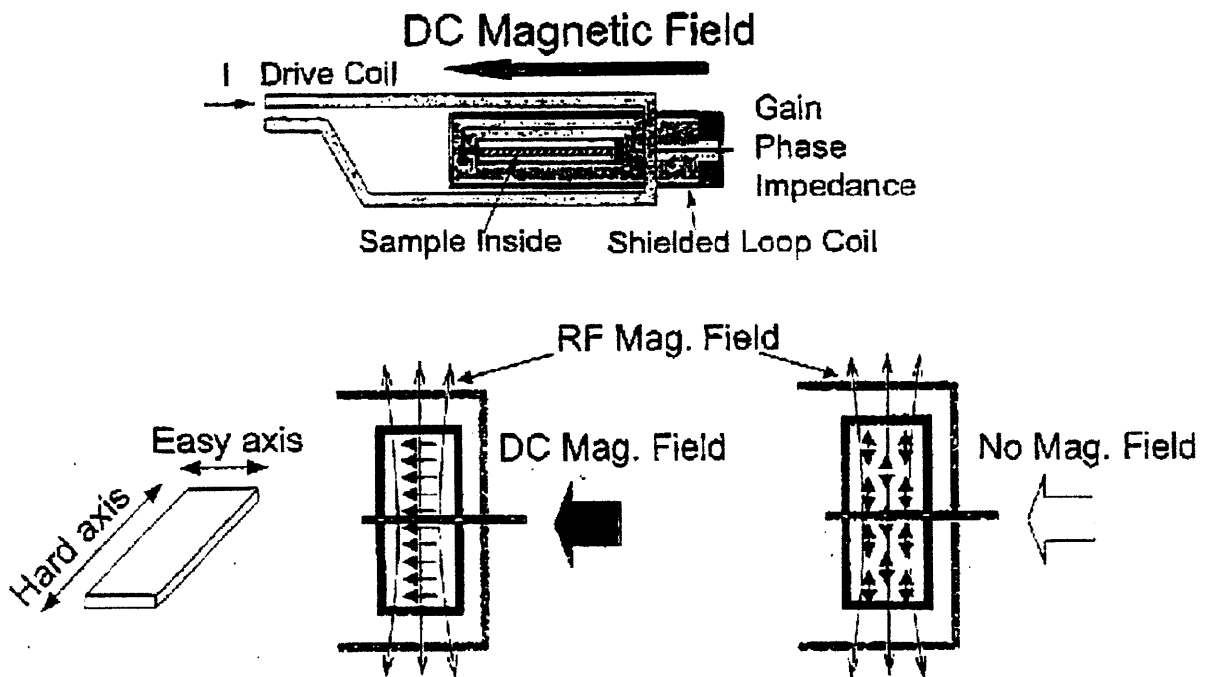Easy axis

Hard axis

DC Mag. Field

No Mag. Field

Figure 2.17 Principle measurement of Ryowa PMF-300 [34]

This equipment capable to measured the magnetic permeability from 1MHz to 3GHz. The Parameter from the hysteresis curve such as magnetic saturations and anisotropic magnetic field strength H_k is necessary as input. The Data of magnetic saturations Ms Parameter necessary for the relative permeability calculations, and the anisotropic magnetic field strength H_k is for Absolute corrections of the equipments.

The obtained results was in standard format, permeability, μ Vs frequency (1 MHz – 3 GHz)

2.11   Return loss, RL measurements.

2.11.1   Equipment

Return loss measurement was conducted by using Hewlett Packard (HP) 8722D Network analyzer. This equipment able to measured up to 10 GHz or higher. The Scattering parameter or also known as "S" parameter was obtained used to perform the RL measurement.

The calculations was based on the equations below,

$$RL = 20 \log_{10} S_{11}$$

Which is S_{11} is the input port voltage reflection coefficient. S11 parameter can be obtained by 1 port coaxial cable.

2.11.2 Specimens for Return loss, RL measurements

The objective are to determine the effect of woody shape ferrite, therefore the microstructure of specimens was shaped into few conditions. Instead of woody microstructures, the non-wood microstructure was produced. To ensure the measurement only related with the pores directions/ geometries the similar bulk density of specimens was prepared. That means, with the same size of specimens it have a similar amount of ferrite. This is because the bulk density influenced the magnetic permeability. The grains are also in similar size because of equal preparation temperature. Figure 2.18 (a)-(d) shows the toroid specimens with different microstructures.
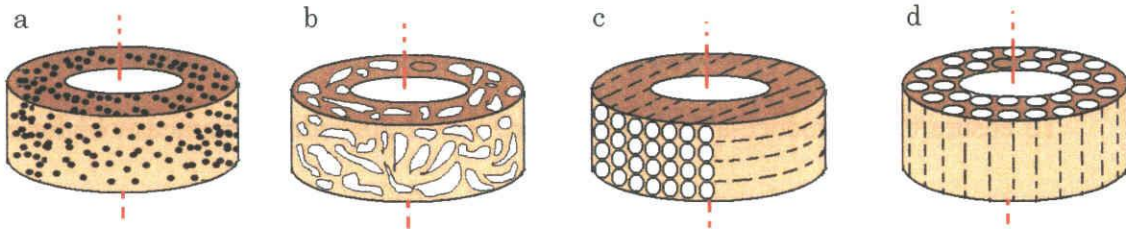

Figure 2.18 the toroid specimens with different microstructures (a) $Ni_{0.5}Zn_{0.5}Fe_2O_4$ powder (b) non-woody microstructure ferrite (c) ferrite wood with horizontal pores and (d) ferrite wood with vertical pores. (All specimens subjected with similar bulk density)

The toroidal shape specimens with diameter 7mm, inner diameter 3mm and thickness 2.5 mm was required for this experiment. Figure 2.19 shows the specimen and the sample holder for measurement of S11 parameter by using single port. To produce thus specimens the non-magnetic polymer binder is necessary to be applied to enhance the toughness.
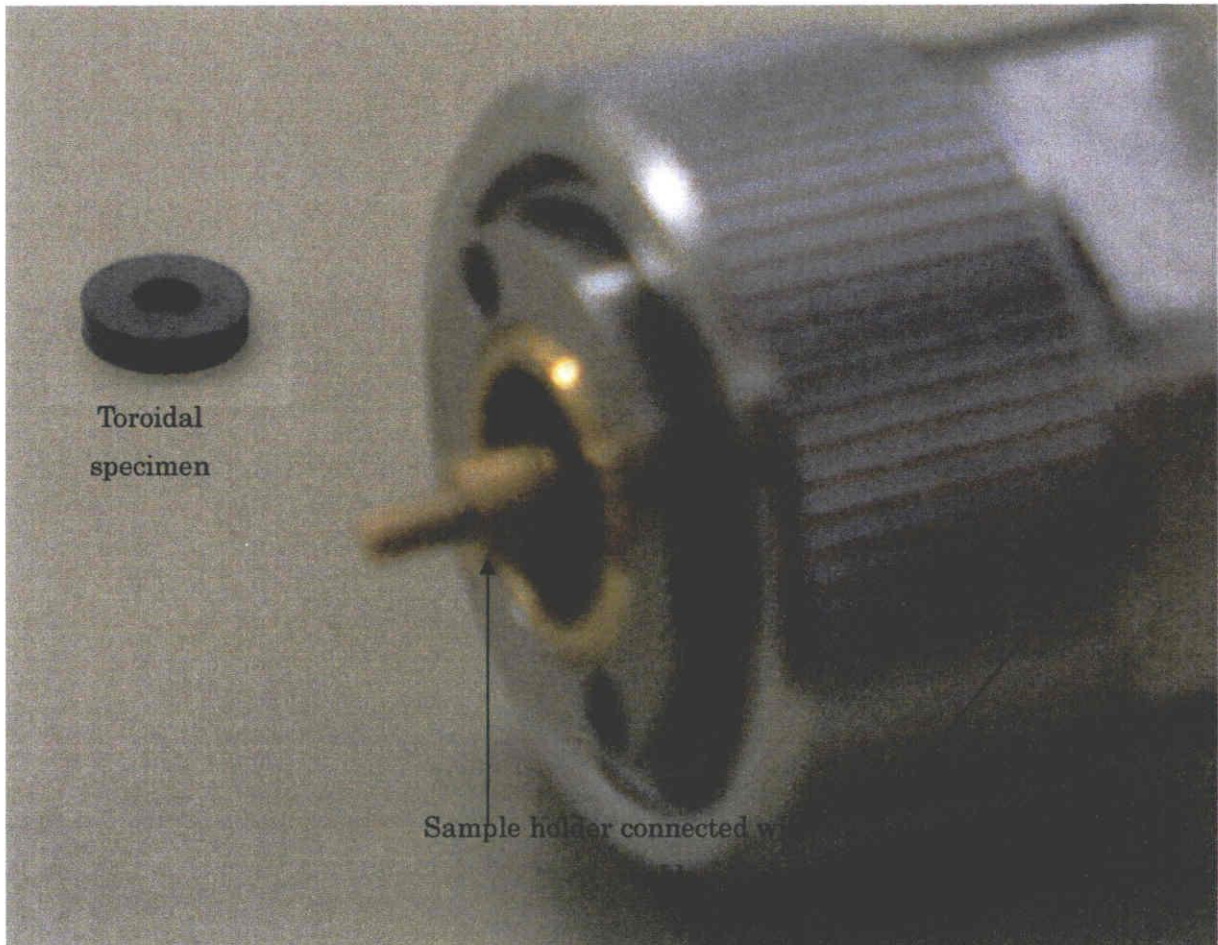
Figure 2.19, Specimen and the Sample holder for 1 port S_{11} parameter measurements.

To ensure the reproduce-able results, more than 1 specimen was measured for each set of microstructure.

CHAPTER 3

PREPARATIONS OF FERRITE WOODS

3.1 Introductions

In this chapter the preparations method of ferrite woods were presented. The Soft ferrite

and hard ferrites attempted. Which are;

1.   Soft ferrite

-     Ni-Zn ferrite wood

-     Mn-Zn ferrite wood

2.   Hard ferrite

-     Ba ferrite wood.

The preparation methods for each ferrite wood were different due to the

chemical different for each composition. The transformations mechanism for each

ferrite wood was examined by using DT-TGA analysis.

3.2   Mechanism Transformations into NiZn ferrite wood

3.2.1   Differential thermal analysis DTA and Thermogravimetric Analysis TGA (Ni-Zn ferrite)

Thermal Analysis of cedar template that infiltrated with precursor (section

2.2.2) was performed in heating rate $10^{\circ}C/min$ (Rt $-$ $1200^{\circ}C$) with a standard reference

Al_2O_3. Thermal study shows that there are few endothermic peaks and more exothermal

peaks were reveals (figure 3.1). From thus peak it was divided into few phase. First

phase endothermic peak ($\sim$ $100^{\circ}C$) probably due to the removal of wet [36] or

dehydration [18]. In this region the weight loss was lesser than reported [36] because the template was dried. The second phase (exothermic ~120°C - ~ 190°C) was energy released due to the decomposition of mixed starting material (Ni, Zn and Fe) Nitrate and the similar pattern of weight loss were found as figure 3.3 In figure the DT-TGA shows only 2 endothermic peaks that represent the decompositions and crystallizations mechanism. At ~ 260°C the wood organic such as hemicellulose, cellulose and lignin this is agreed by [36] due to the rapid weight loss. And next stage with the temperature at 290°C – 330°C presumably attributed to crystallizations of the Nitrate into Iron Oxide form. The XRD pattern in figure 3.4 indicates the crystallizations of the (Ni, Zn and Fe) Nitrate into Oxide form at 330°C. This XRD pattern shows the peak of –Fe_2O_4 and Fe_2O_3 were become more intents by increased of the temperature. And finally at 340°C – 400°C the oxidations decomposition involving the biopolymetric oxygen and breakdown of the C chains of the polynuclear carbon structure of wood organic and reacted with air and might released into air as Gas form (CO_2 or CO). figure 3.2 shows the DT-TGA for cedar wood that conducted as the same conditions, the TG curve it show that the almost all the wood component disappear at 550°C. Meanwhile for infiltrated template, it seems like the reach the steady state losses at 400°C. This might be due to the existing of Nitrate that accelerates the firing of wood component. The peak was covered at temperature 400°C – 1200°C. This peak might be due to the existence of phase changes of – Fe_2O_3 (hematite) and some -Fe_2O_4 (ferrite). Meanwhile this endothermic peak was covered by large range of temperature probably due to the reaction times. This can explained by the most conventional method preparation of Ni-Zn ferrite will consume longer time at target temperature. This analysis found that ~16% weight remained (~84% loss) at 1200°C because removal of the wood organic.
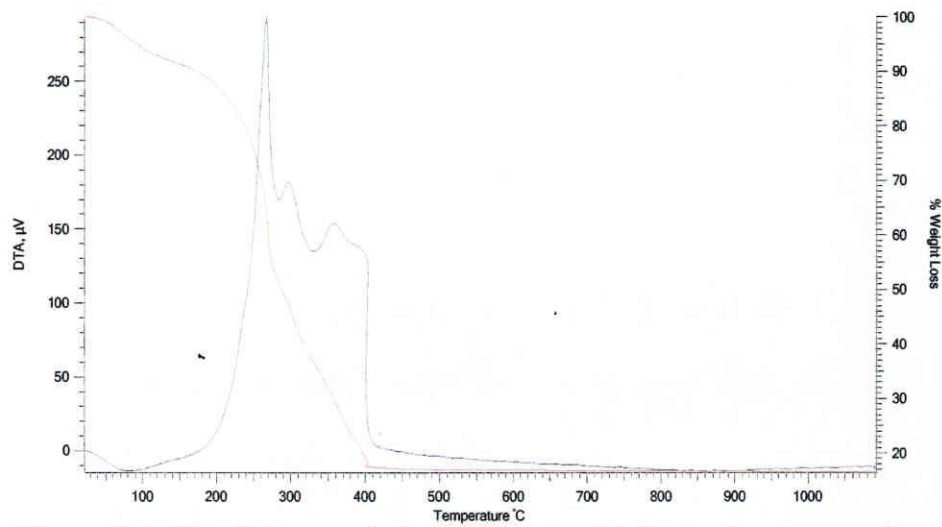
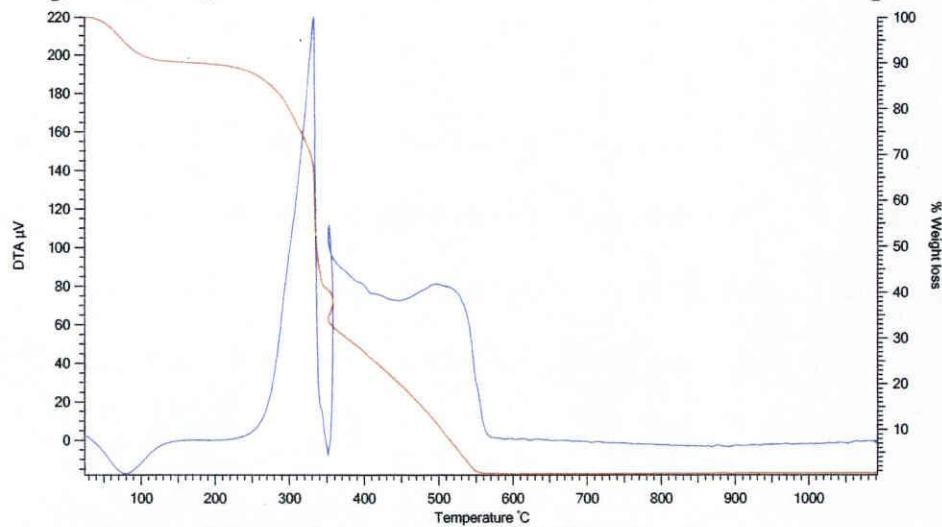Figure 3.1 TG, DTA recorded at 10°C/min of infiltrated cedar template

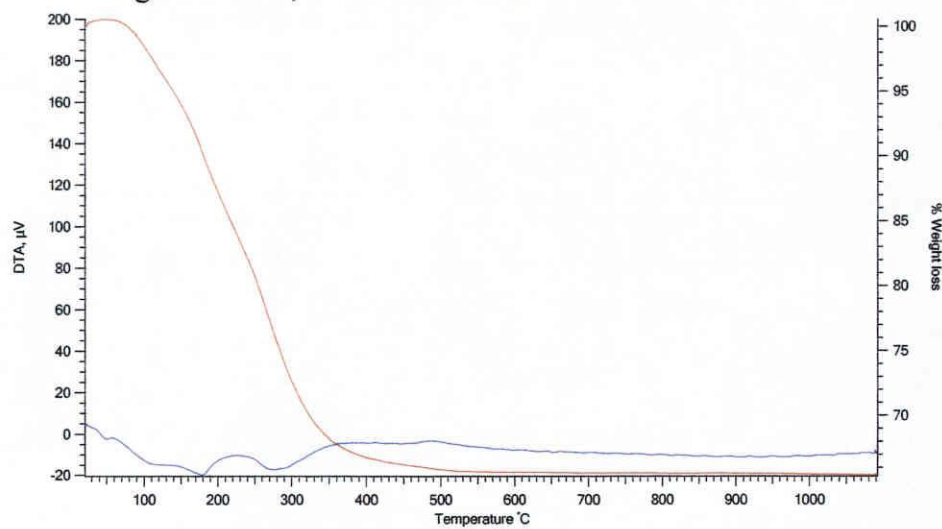Figure 3.2 TG, DTA recorded at 10°C/min of cedar wood

Figure 3.3 TG, DTA recorded at 10°C/min dried Mixed (Ni-Nitrate, Zn-Nitrate and Iron Nitrate)
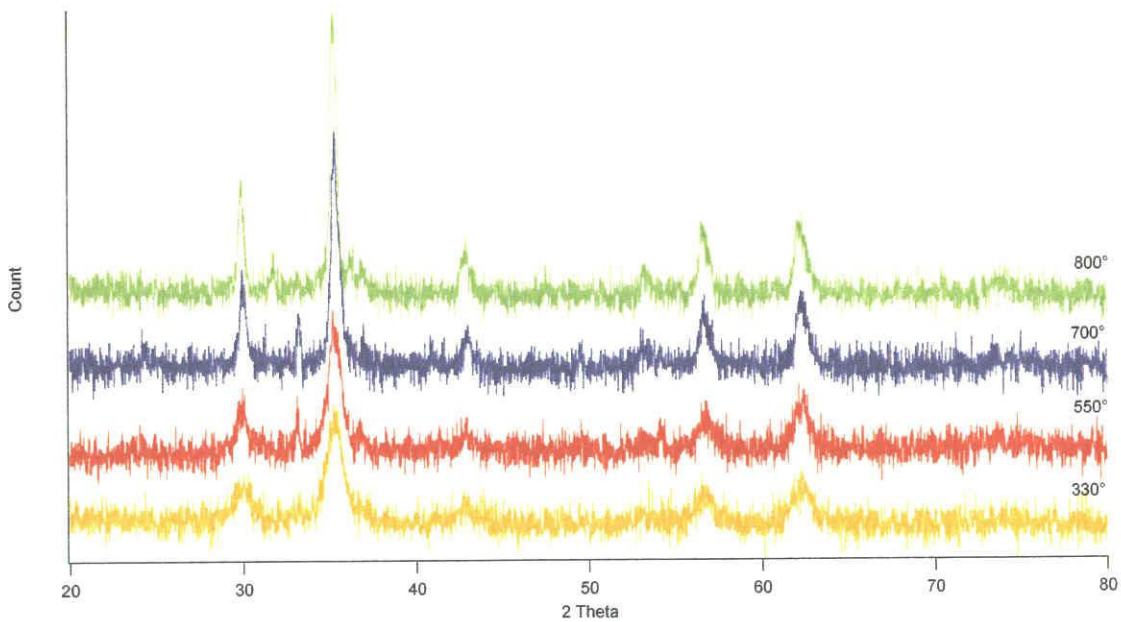
Figure 3.4 XRD pattern of Template sintered in air

3.2.2 Summarization of Infiltrated wood – ferrite wood transformations

The ferrite wood retained the shape of the template because the crystallizations of Ni + Zn into iron oxide form at lower temperature than firing of wood. Figure 3.5 summarizes the transformations process.
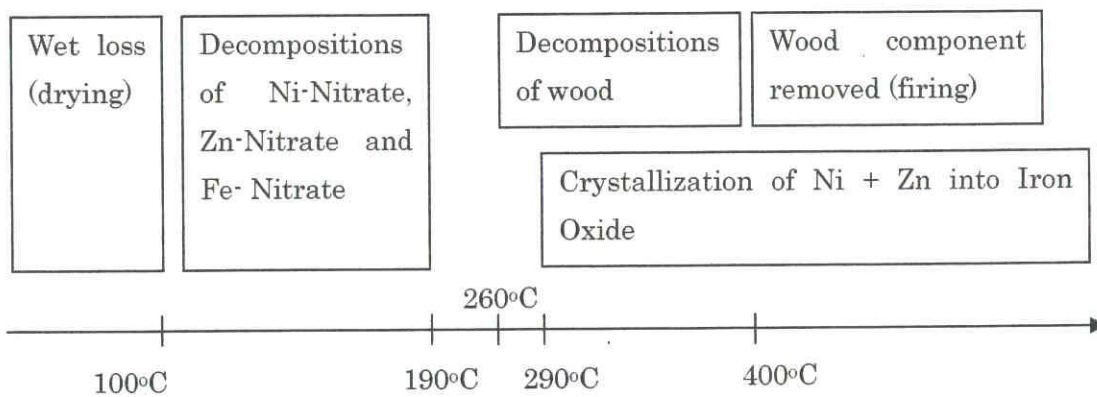

Figure 3.5 summarize the transformations process of infiltrated woods into ferrite wood

3.3 Single Phase $Ni_{0.5}Zn_{0.5}Fe_2O_4$

The template was sintered in various sets of temperature. At the lower temperature the single phase Ni-Zn ferrite didn't form. The ZnO, NiO, Fe_2O_3 and etc still remained. Various sintered temperatures and sintered times was attempted. Figure 3.6 shows the XRD pattern that sintered with various temperatures ($1050^{\circ}C$ -$1400^{\circ}C$) for 2h, the peaks become intense and thinner. This argument agreed by M. Jalaly et al [37] that successfully $Ni_{0.3}Zn_{0.7}Fe_2O_4$. The pattern indicates that the hematite peak disappeared at $1400^{\circ}C$ and only typical spinel ferrite peak revealed. The XRD pattern indicates the single phase only form at the higher temperature or longer sintering time. Meanwhile figure 3.7 shows the 8 h sintering time for $1000^{\circ}C$ – $1300^{\circ}C$ and the single phase was revealed at lower temperature ($1200^{\circ}C$). The similar set of sintering temperature for 1 h and 6 h was conducted. The result was concluded at Table 3.1 that stated the existing phase for every set of sintered time / temperature.
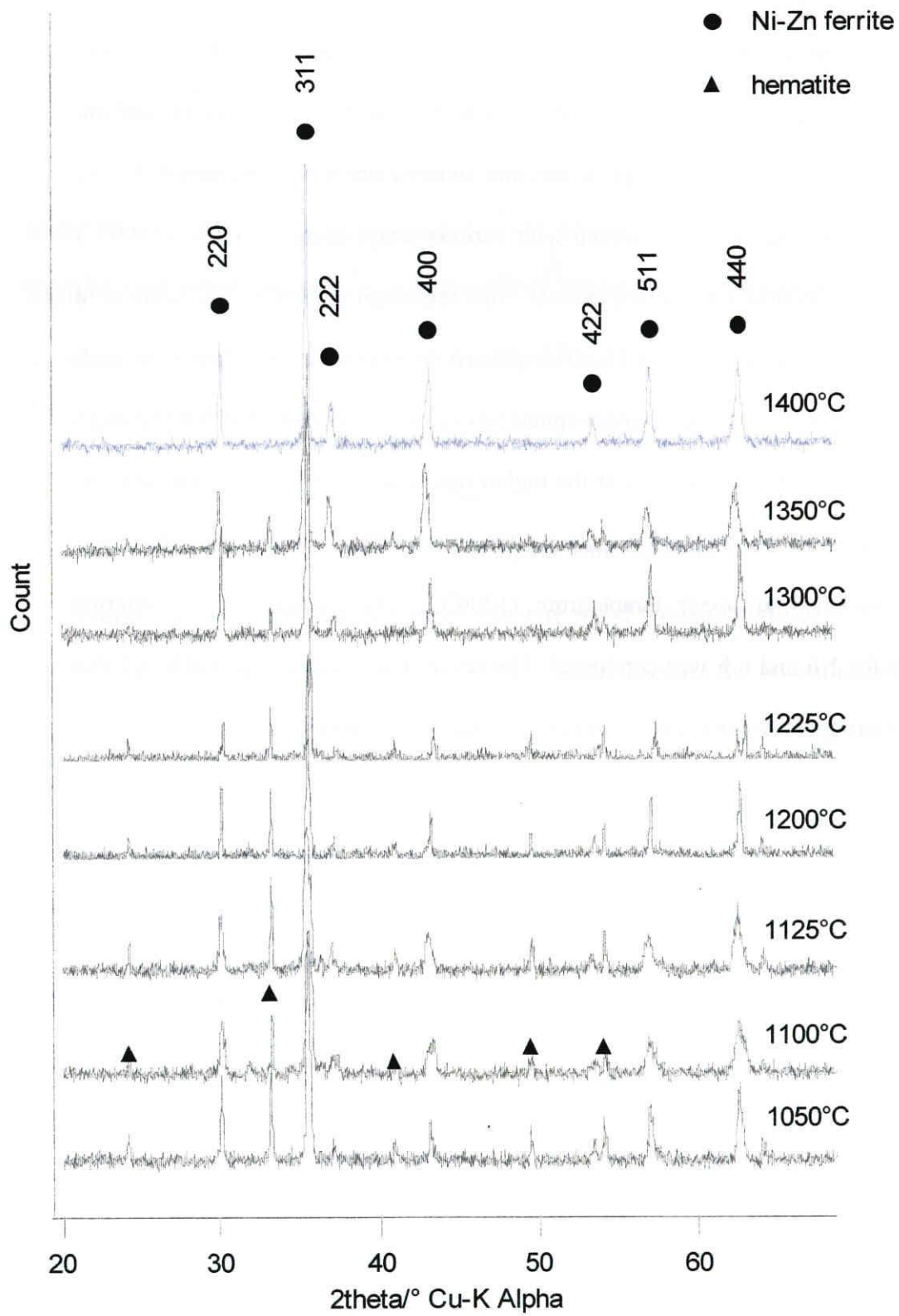
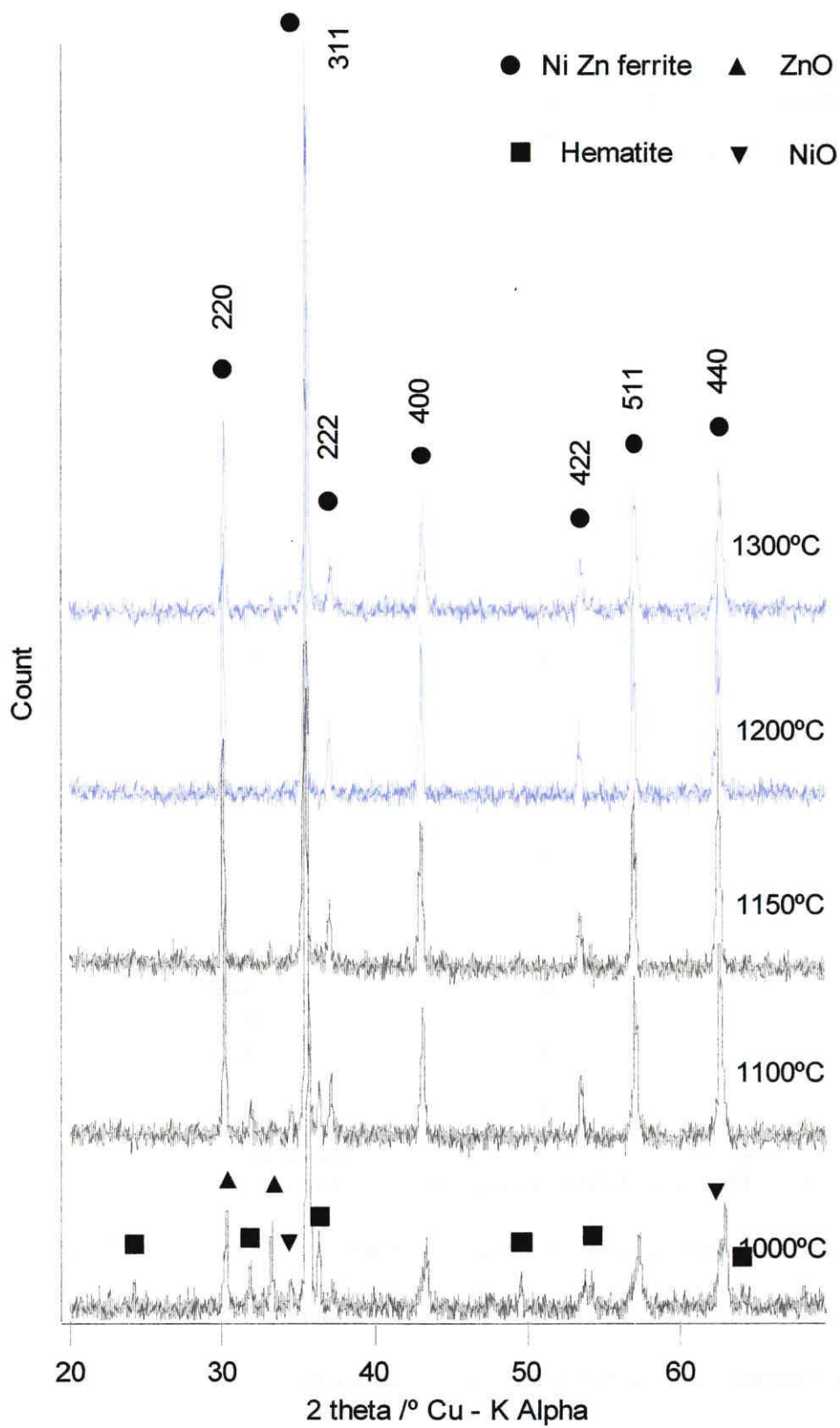Figure 3.6, Infiltrated template that sintered for 2h.

Figure 3.7 Infiltrated templates that sintered for 8h

Table 3.1 The existed phase for various sintering temperature and time.

Sintering temperature °C	Sintering time h	Phases exist *
1000	8	H+NZF+O
1050	2	H+NZF
1100	2	H+NZF
	8	H+NZF
1125	2	H+NZF
1150	8	H+NZF
1200	2	H+NZF
	8	NZF
1225	2	H+NZF
1300	2	H+NZF
	8	NZF
1350	2	H+NZF
	6	NZF
1400	2	NZF
1500	1	NZF

* H= Hematite, NZF=Ni-Zn ferrite, O= Others

By increasing the sintering temperature and sintering time the color was change from brown to black. This might be the hematite were color of hematite that exists at the lower temperature. Sintered at the lower temperature need a longer time for the single phase $Ni_{0.5}Zn_{0.5}$ ferrite formed. Table 3.1 shows the sintered temperature times and phase that revealed. Sintered at the lower temperature, the Hematite exists. Sintered at

1500°C the single phase of $Ni_{0.5}Zn_{0.5}Fe_2O_4$ form and by decreasing the sintering temperature the longer time was necessary. Figure 3.8 shows the curve of sintering temperature vs sintering times.
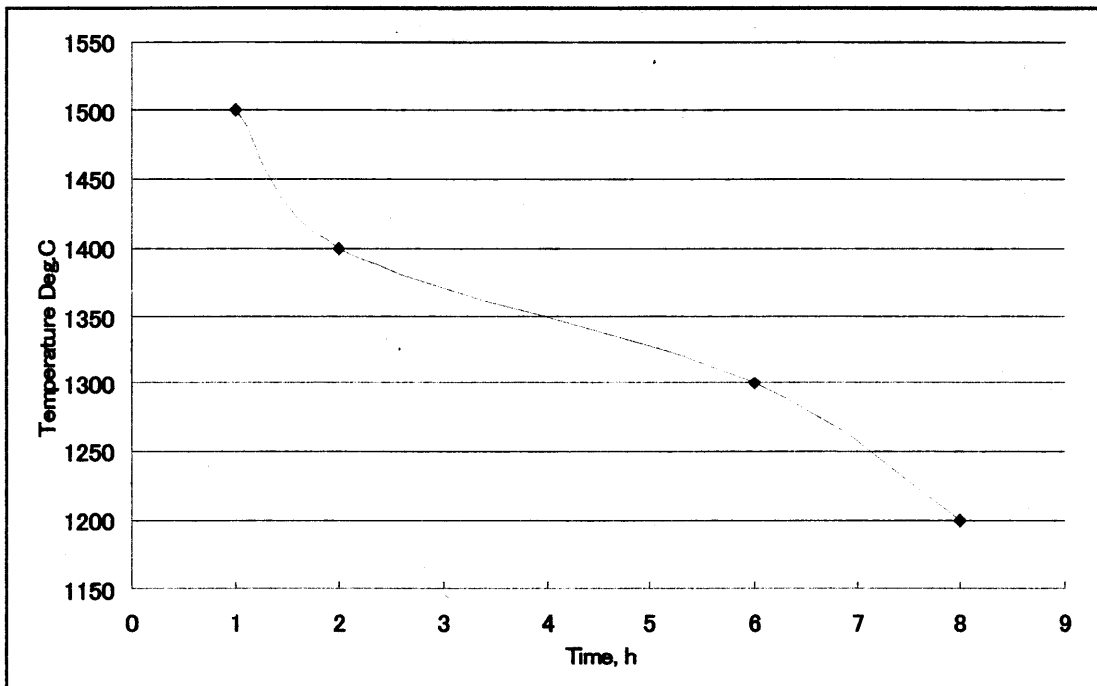

Figure 3.8 Transformation curve of Single phase $Ni_{0.5}Zn_{0.5}$ ferrite

3.4 Sintering time effect

But by sintering at the higher temperature the shape of specimens were highly defected. Figure 3.9 shows the shape of the $Ni_{0.5}Zn_{0.5}Fe_2O_4$ that sintered at 1200°C for 8h and 1500°C for 1h. For highly defected specimens, the wood microstructure was not found. The specimens that sintered at 1200°C for 8h are in good shape with a minimum defect. The reason this phenomenon occurred because of sintered at higher temperature caused the grain growth and the pores contracted. In additions sintered in longer time is necessary in preparing the ferrite wood to ensure the removal of wood organic.
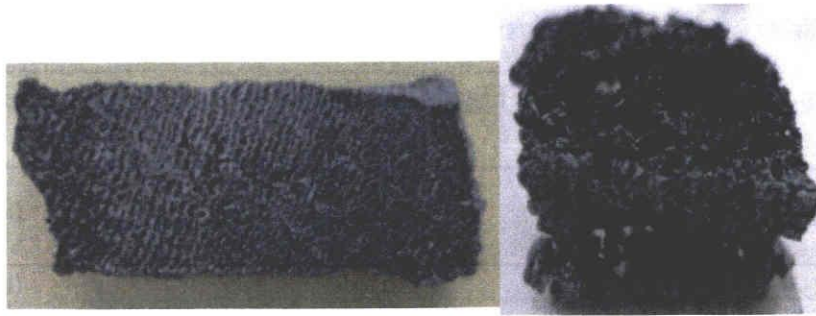
Figure 3.9 $Ni_{0.5}Zn_{0.5}$ ferrite sintered at (a). $1200^{\circ}C$ for 8h and (b) $1500^{\circ}C$ for 1h.

3.5   Optimum preparation of $Ni_{0.5}Zn_{0.5}Fe_2O_4$ from wood template

The optimum preparation of $Ni_{0.5}Zn_{0.5}Fe_2O_4$ from wood template was judged by the shape of specimens, composition contain and microstructure. Thus aspect was controlled by the Infiltrations time, sintering temperature and the sintering time. After considering thus aspect, the optimum preparation of $Ni_{0.5}Zn_{0.5}Fe_2O_4$ from wood template was summarized in the table below.

Table 3.2 The optimum preparation condition of preparation of $Ni_{0.5}Zn_{0.5}Fe_2O_4$ from wood template

Infiltration time	at least 7 days
Sintering temperature	$1200^{\circ}C$
Sintering time	8h
Template thickness.	< 15mm

3.6   Preparations of $Ni_xZn_{1-x}Fe_2O_4$ from wood template (X = 0.1,0.5 and 0.9)

After determined the optimum preparation of $Ni_{0.5}Zn_{0.5}Fe_2O_4$ from wood template, the preparation of Ni-Zn ferrite with the different amount of Ni^{2+} and Zn^{2+} were conducted. The stoichiometirc proportions were stated in table 2.1 (Chapter 2).

The optimum preparation method also applicable with the $Ni_xZn_{1-x}Fe_2O_4$ from wood template (x = 0.1 and 0.9).

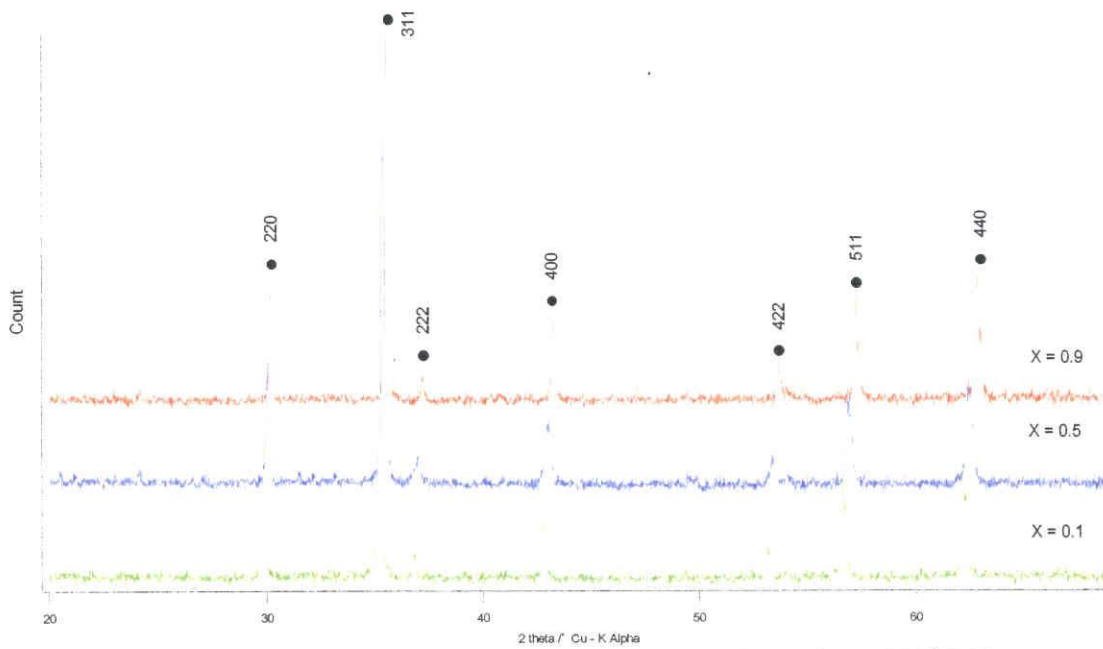## 3.6.1 XRD pattern of $Ni_xZn_{1-x}Fe_2O_4$ from wood template (X = 0.1, 0.5 and 0.9)

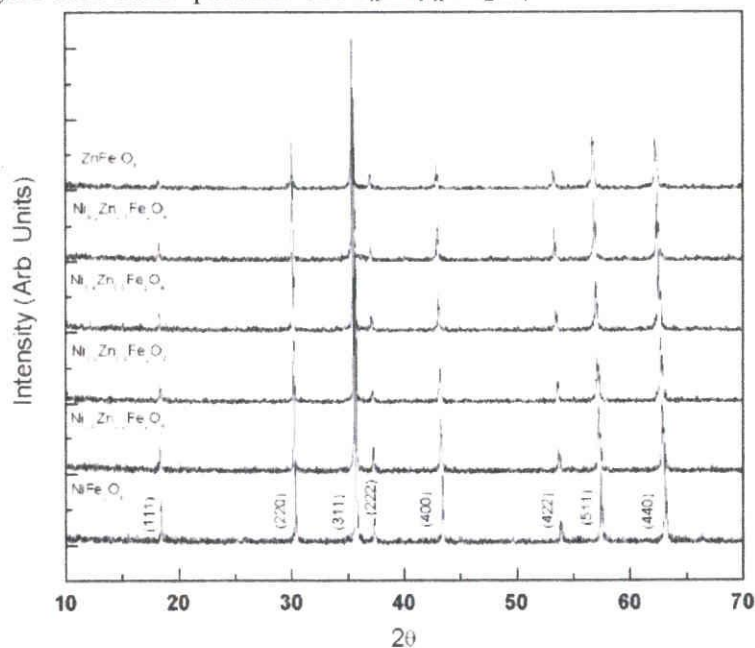Figure 3.10 XRD patterns of $Ni_xZn_{1-x}Fe_2O_4$ sintered at $1200^{\circ}C$ 8h

Figure 3.11 XRD of Ni - Zn ferrites using conventional sintered method [28],

51

XRD pattern (figure 3.10) shows only the spinel ferrite peaks obviously have a high count of intensity. But by increasing the amount of Ni^{2+} the peak was shifted to the higher angle. This argument are correspond with the reported [28] (figure 3.11) that prepared by conventional sintering method.

The peaks were shifted because of the crystal structure expansion due to substitution of smaller Ni ions in place of bigger Zn ions in the $Ni_xZn_{1-x}Fe_2O_4$ structure. As reported earlier, the Ni^{2+} ions prefer octahedral sites because of their favorable alignment of charges in the octahedral site's crystal field. The peak shifts to higher diffraction angles with increasing x. Since the ionic radius of Zn^{2+} (0.82 A) is larger than that of Ni^{2+} (0.78 A) the lattice parameter become smaller.

3.6.2 Lattice of Ni-Zn Ferrite Wood

Tables 3.3 show the calculated lattice parameter of $Ni_xZn_{1-x}Fe_2O_4$ via XRD pattern obtained in previous section. All peaks have an intensity at least 29% referring to the peak 311. The different of the lattice calculate might be due to the large diffractometer angle (0.02°) for every measurement. That means for small angle might caused a big different (Sensitive of small angle change), example for x= 0.1 peak 2 2 0 if 2θ = 29.89° ($\Delta 0.01°$) the lattice will be change to 8.444 Å. Therefore to minimize thus effect, the highest angle peak (peak 440) was chosen as a lattice constant.

Table 3.3 The calculated lattice parameter of $Ni_xZn_{1-x}Fe_2O_4$ via XRD pattern

X = 0.1

2θ	d	i/i_o	h	k	l	a (Å)
29.90	2.985	52	2	2	0	8.442
35.22	2.545	100	3	1	1	8.441

36.84	2.437	29	2	2	2	8.441
42.80	2.110	35	4	0	0	8.441
53.10	1.723	31	4	2	2	8.439
56.60	1.624	44	5	1	1	8.439
62.14	1.492	47	4	4	0	**8.440**

X=0.5

2θ	d	i/i_o	h	k	l	a (Å)
30.04	2.971	55	2	2	0	8.403
35.40	2.532	100	3	1	1	8.399
37.04	2.424	34	2	2	2	8.397
43.04	2.099	42	4	0	0	8.396
53.38	1.714	34	4	2	2	8.398
56.86	1.617	46	5	1	1	8.404
62.44	1.485	50	4	4	0	**8.403**

X=0.9

2θ	d	i/i_o	h	k	l	a (Å)
30.20	2.956	48	2	2	0	8.360
35.58	2.520	100	3	1	1	8.358
37.20	2.414	32	2	2	2	8.362

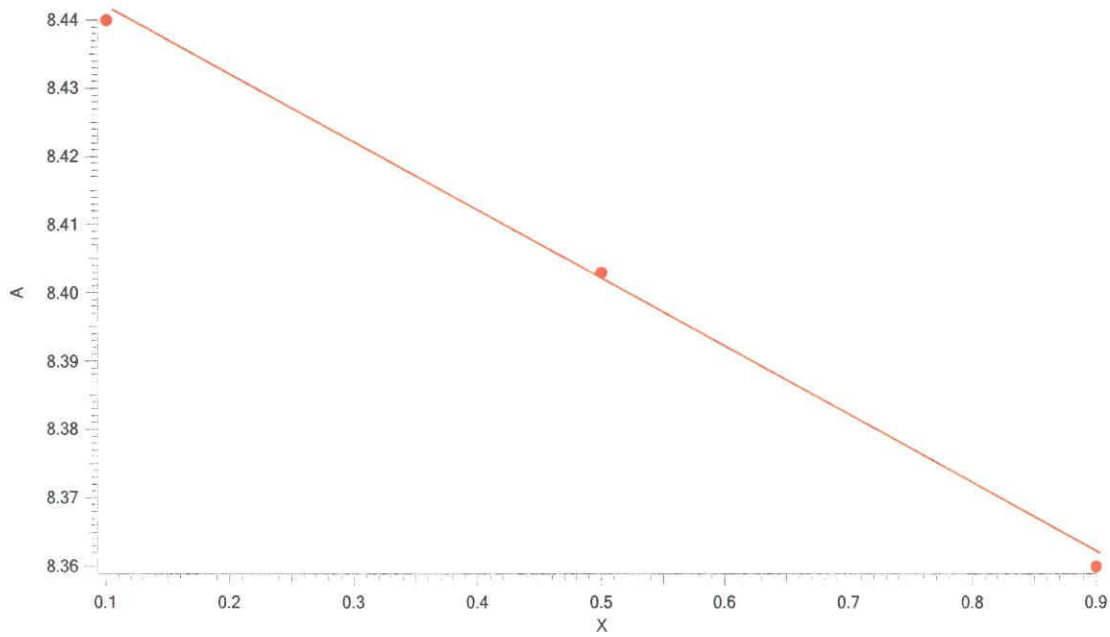| 43.24	2.090	43	4	0	0	8.359
53.66	1.706	34	4	2	2	8.357
57.20	1.608	45	5	1	1	8.358
62.80	1.478	49	4	4	0	**8.360**

Figure 3.12 Lattice constant as function of x for $Ni_xZn_{1-x}Fe_2O_4$
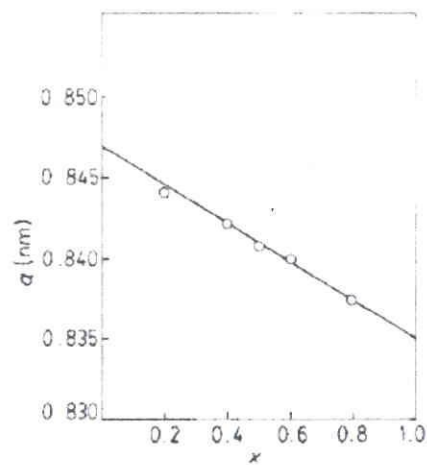

Figure 3.13 Variation of lattice constant as function of x in $Ni_xZn_{1-x}Fe_2O_4$ .Adapted from [2]

Figure 3.12 shows the lattice parameter in the function of composition. In the case of $Ni_xZn_{1-x}Fe_2O_4$ the rich Zn^{2+} spinel have a smaller lattice. P. Ravindranathan [38] was also reported the small different value of the lattice (figure 3.13). This is because at higher temperature, it leads to grain growth which affected the particle size as well as ionic distributions [17]. That caused by some ion either Ni^{2+} or Zn^{2+} that occupied the tetrahedral and octahedral site of mixed spinel. The changing site for each ion affected the lattice constant. This situation can be explained by equations below.

$$Ni_\gamma Zn_\delta Fe_{1-\gamma-\delta}\left[Ni_{x-y}Zn_{1-x-\delta}Fe_{1+\gamma+\delta}\right]O_4$$
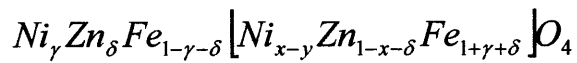
The distribution of the cation in tetrahedral and octahedral will influence the magnetization in the rich Ni^{2+} region due to the net moment that produce by parallel and anti- parallel fashion.

3.7   SEM images of Ni-Zn ferrite wood

Figure 3.14 (a) shows the cedar templates and (b) was a Ni-Zn ferrite wood that sintered at 1200°C for 8h. Most of the woody microstructures were retained. From the figure, indicates some of the sintered body was deformed and the pores have inhomogeneous sizes.
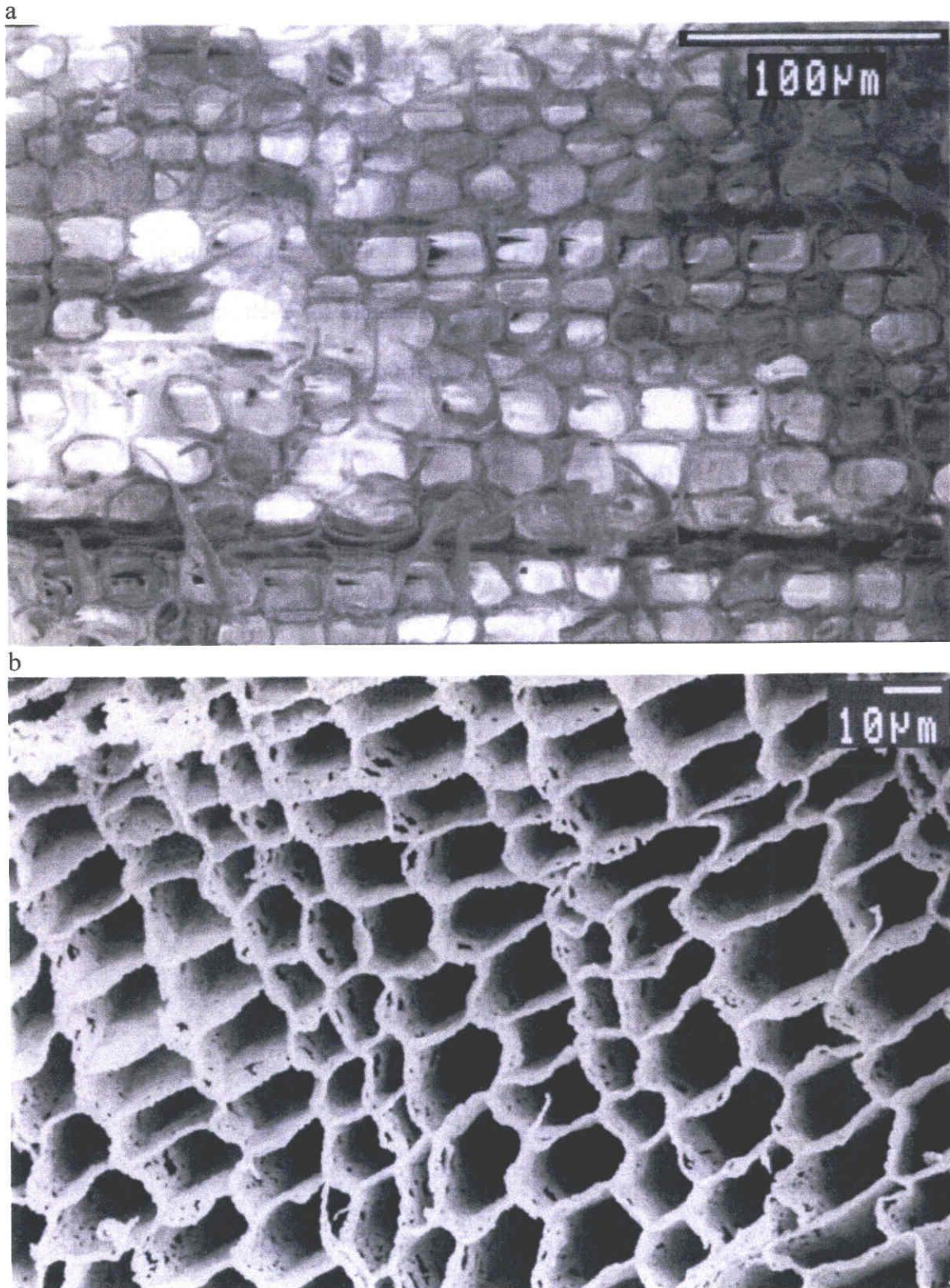
Figure 3.14 a. Microstructure of cedar template and b. Ni-Zn ferrite wood

Figure 3.15 – 3.17 shows the $Ni_x Zn_{1-x}Fe_2O_4$ (x = 0.1, 0.5, 0.9) from cedar

template. It seem like by increasing contain of Zn^{2+} were caused the increasing of grain

sizes. The microstructure of the cedar template retained. The ferrite woods were mimicking the wood microstructure which is constructed by a multiple layer of sintered body that arrayed like checker board shape. Consequently, contribute to the 1 directional pores.
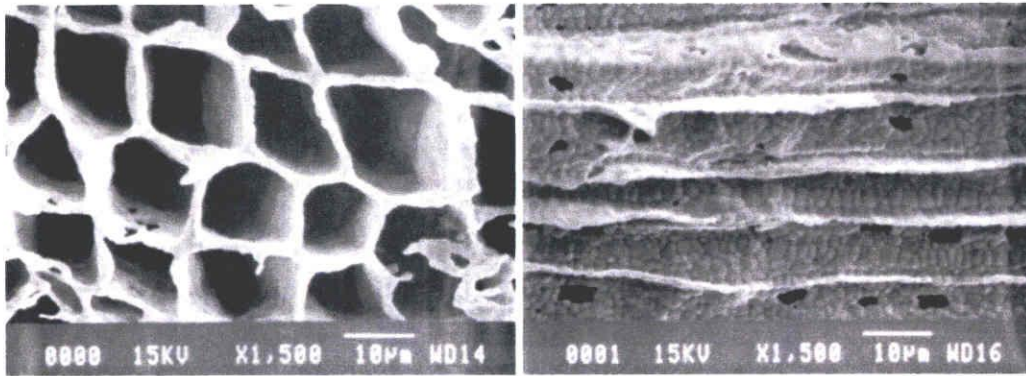

Figure 3.15 microstructure of $Ni_{0.1}Zn_{0.9}Fe_2O_4$ from cedar template. a) fron view, b)side view
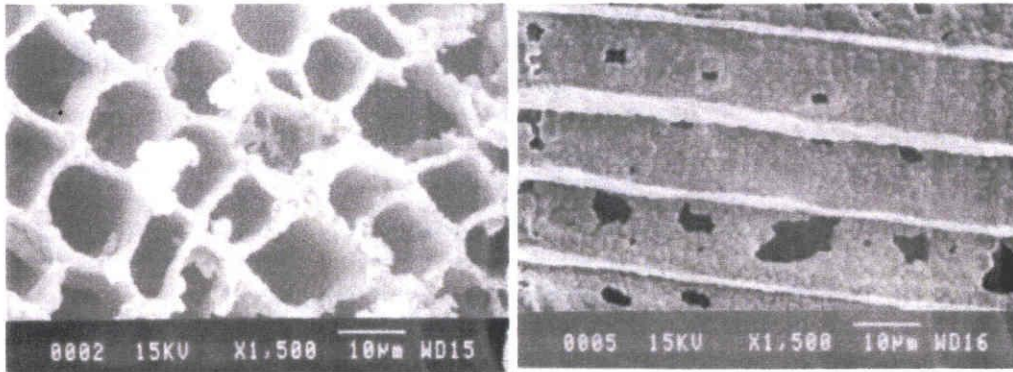

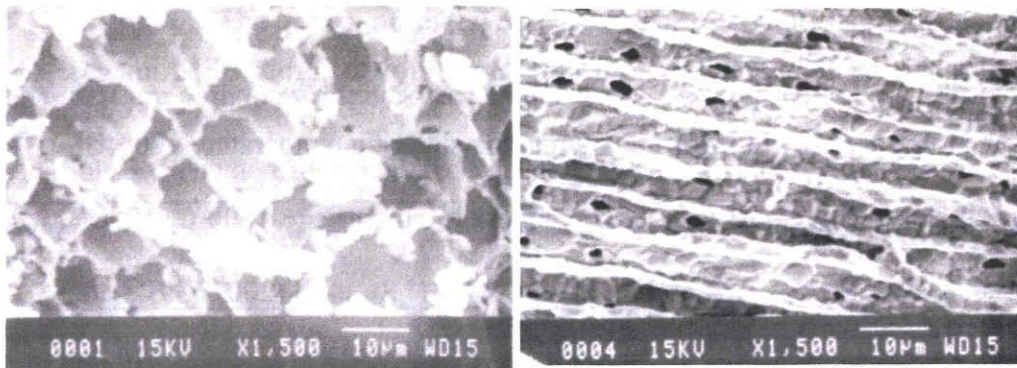Figure 3.16 microstructure of $Ni_{0.5}Zn_{0.5}Fe_2O_4$ from cedar template. a) fron view, b)side view

Figure 3.17 microstructure of $Ni_{0.9}Zn_{0.1}Fe_2O_4$ from cedar template. a) fron view, b)side view

The original cedar templates have larger pores sizes. Sintered at the 1200°C for 8 h cause higher rate of shrinkages because of the porosity. The transformations of the wood to the ferrite wood change the microstructures from bigger pores to smaller pores sizes (figure 3.18).
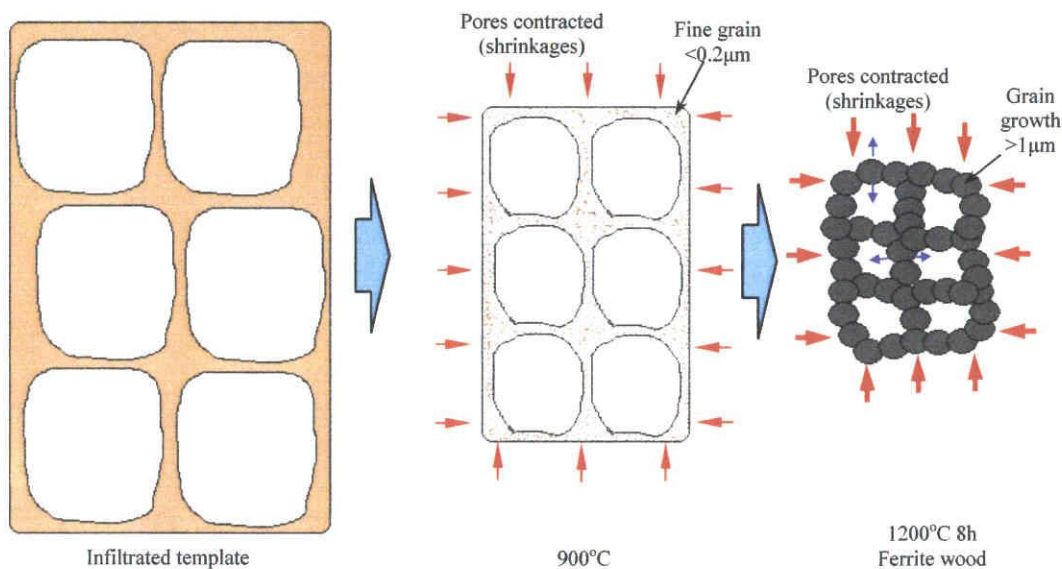

Figure 3.18, Transformation of cedar template into ferrite wood

3.8   Properties of Ni-Zn ferrite wood

3.8.1   Grains sizes

Sintered at higher temperature caused the grain growth. From SEM images, indicates that the grains are growth from $1 - 4$ μm at the sintering temperature 1200°C – 1300°C. Table 3.4 shows the grain sizes for the sintering temperature 1200°C, 1250°C and 1300°C for $Ni_{0.5}Zn_{0.5}Fe_2O_4$. This results agreed with H.Su et al.(2007)[39] stated that the grain growth for Ni-Zn ferrite at 1200-1300°C is not so obvious compared with others material such as NiCuZn ferrite.

Table 3.4 Grain size of $Ni_{0.5}Zn_{0.5}Fe_2O_4$ wood that sintered at $1200°C$, $1250°C$ and $1300°C$

Sintered temperature (°C)	1200	1250	1300
Grain sizes (μm)	1-1.5	1.5-2	2-4

3.8.2 Porosity and Density of Ni-Zn ferrite wood

Table 3.5 shows the results of density measured experimentally (section 2.4). The bulk density of ferrite woods were increase by increasing of sintering temperature. The porosities were estimated around 78 – 88%.

Table 3.5 The bulk density of ferrite wood sintered in 1200 – 1300°C

Sintering temperature °C	specimens	Density g/cc	Porosity(%)
1200	1	0.664	87.5
	2	0.646	87.8
1250	1	0.764	85.6
·	2	0.749	85.9
1300	1	0.851	83.9
	2	1.15	78.3

The results measured bulk densities are applicable due to the confirmation via SEM images. Figure 3.19 shows the SEM images of Ferrite wood that sintered at 1200°C – 1300°C. The pores of the wood assumed in round shape with average diameter 8-10μm with the wall thickness around 1- 4μm.

Table 3.6 The density calculated via average value from SEM images.

Sintering Temp	wall thickness,t	average diameter, D_{avg}	(Bulk density)
1200°C	1.0-1.5μm	10μm	0.504 – 0.737g/cc
1250°C	1.5-2μm	10μm	0.737 - 0.849g/cc
1300°C	2 – 4μm	9.5μm	0.849 - 1.354g/cc

The measured and calculated values of the bulk densities were corresponded. For the calculated results (table 3.6) shows that at higher sinter temperature caused larger grains size that contribute to the thicker wall.
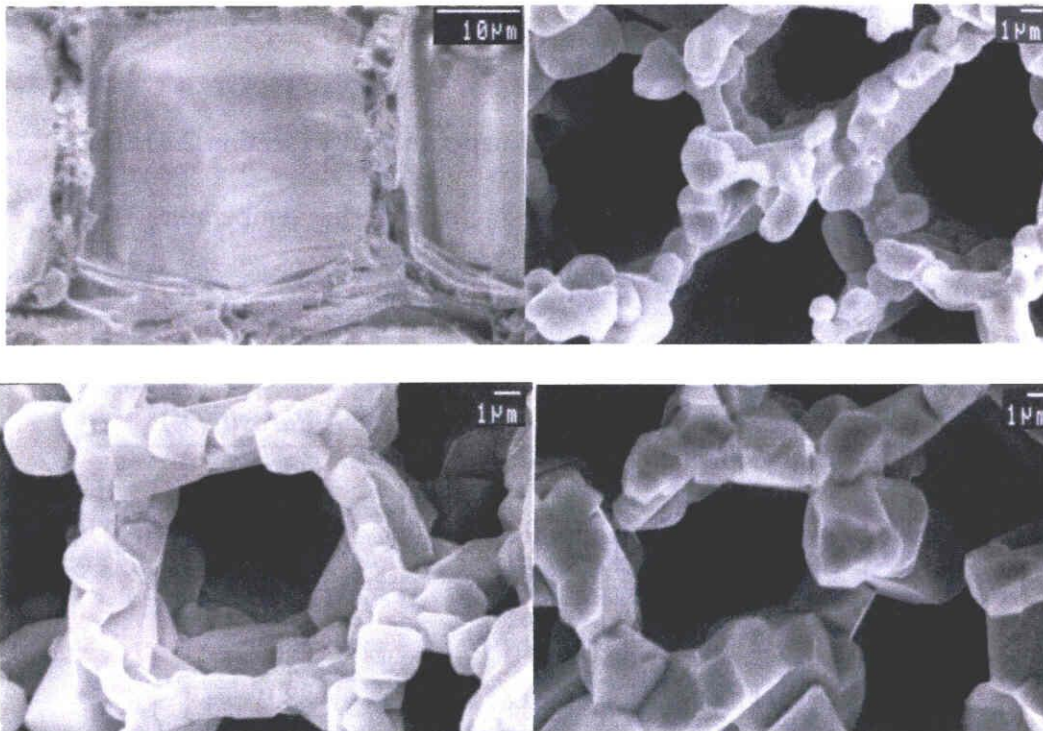

Figure 3.19 Microstructure of (a) cedar template and $Ni_{0.5} Zn_{0.5} Fe_2O_4$ wood sintered at (b) 1200°C, (c) 1250°C and (d) 1300°C

3.8.3 Shrinkages of Ni-Zn ferrite wood

Sintered specimens shrink due to the contracted grain. Porosity is a major factor that contributes to shrinkages. Normally, most of the bulk specimens will shrink equally in all directions because of the homogenous porosity. In order to minimize the shrinkages some study applied some additives. Topfer et al (2006)[40] were use Bi_2O_3 additive for of Ni-Cu-Zn ferrite powder enhance densifications during sintering at 900°C and high densities are obtained (reduce the shrinkages rate). It results shrinkages, dl/l_o(%) that sintered at 1000°C were reduced from -17.5% to -15% (improved 2%). Additive might be easy for apply for powder based material. But to produce ferrite wood, the additive that reduce the shrinkage difficult to apply.

For Ni-Zn ferrite and Mn-Zn ferrite prepared from wood template have a different outcome. It has a very high porosity approximately 78 – 88% (section 2.3). The pores that distributed in 1 directional gave preferences to shrink in perpendicular pores directions (figure 3.20).
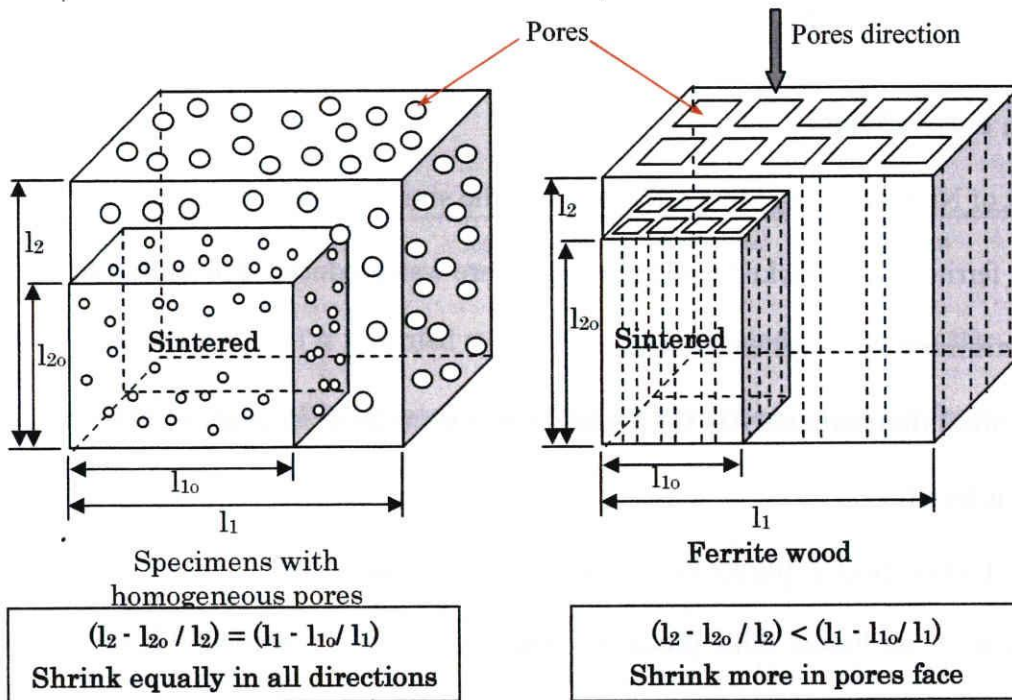

Figure 3.20 shrinkages of specimens with a. homogenous pores distribution, b. 1 directional pores distributions.

Table 3.7 Shrinkages of ferrite wood in pore face sintered at $1200 - 1300^{\circ}C$

Sintering Temperature	average size of template sizes	average size of ferrite wood cell	shrinkages
$1200^{\circ}C$		$\approx 10\mu m$	$\approx 75\%$
$1250^{\circ}C$	$\approx 40\mu m$	$\approx 10\mu m$	$\approx 75\%$
$1300^{\circ}C$		$\approx 10\mu m$	$\approx 75\%$

Table 3.8 Shrinkages of ferrite wood in pore direction sintered at $1200 - 1300^{\circ}C$

Sintering Temperature	high of template	high of ferrite wood	Shrinkages
$1200^{\circ}C$		$\approx 6\text{-}7mm$	$\approx 30\text{-}40\%$
$1250^{\circ}C$	$\approx 10mm$	$\approx 6\ mm$	$\approx 40\%$

1300°C	≈5-6mm	≈40-50%

Table 3.7 and 3.8 shows the results of the shrinkages of the wood specimens in pore face and direction. The high shrinkages occurred in the pores face approximately 75%. Meanwhile in pores direction that measured directly from the template and specimen was shrink at 30 – 50% depend on the sintering temperature.

3.9   Mn-Zn Ferrite Wood

Instead of Ni-Zn ferrites, Mn-Zn ferrites with the similar crystal structure were studied. Mn-Zn ferrite that mimicked wood microstructure was produced. Mn-Zn ferrite with ferrimagnetism behavior was examined.

3.9.1   Differential thermal analysis DTA and Thermogravimetric Analysis TGA (Mn-Zn ferrite)

Thermal analysis of Infiltrated cedar was performed and show in figure 3.43. The specimens were infiltrated with precursor solution (Table 2.1 section 2.2.2). It seems like it have a similar pattern of thermogram and TG curve compared with Ni-Zn ferrite (section). Because of this reason, it was assumed to be the same reaction occurred at the temperature below 500°C. The remained weight was approximately 7% which is lower compared with Ni-Zn ferrite probably due to infiltability and the weight of Mn that lower than Ni. This might change the amount of the existing ionic and slightly influencing the reaction of the Carbon of the template. It also caused the drastic loss of weight was ended at ~ 450°C compared to the Ni-Zn ferrite 405°C because of the exothermic that ended at that temperature.

Figure 3.22 summarized the transformations of infiltrated template into ferrite wood.
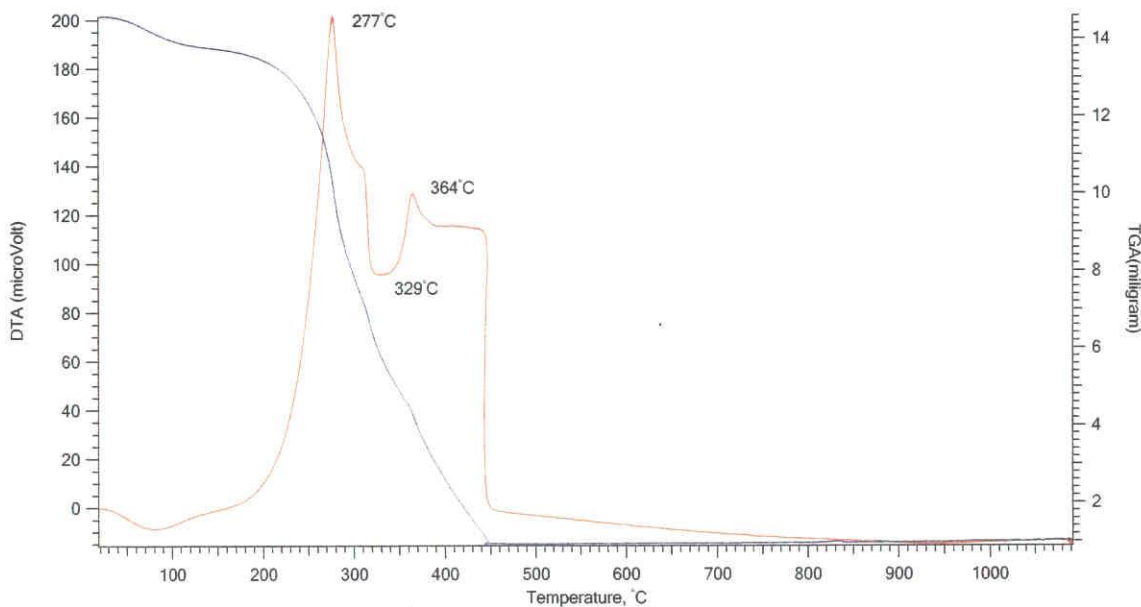
Figure 3.21 TG, DTA recorded at 10^oC/min of infiltrated cedar template

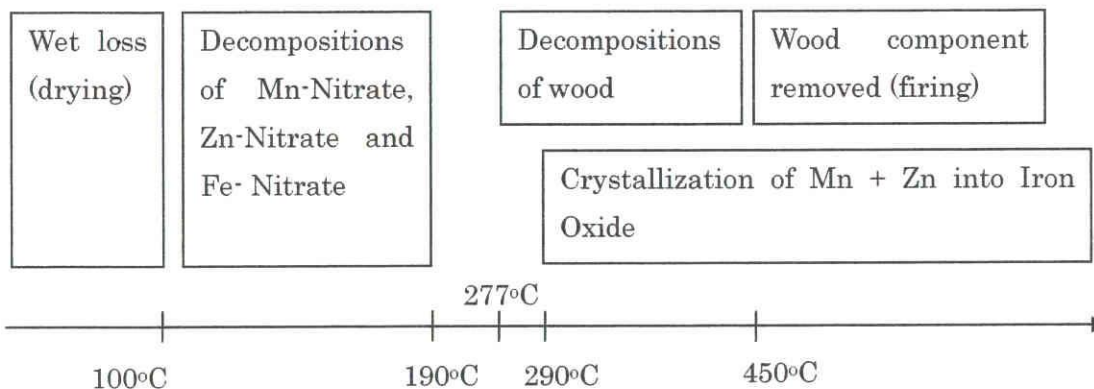**3.9.2 Summarization of Infiltrated wood – Mn-Zn ferrite wood transformations**

Figure 3.22 the transformations process of infiltrated woods into Mn-Zn ferrite wood

The ferrite wood retained the shape of the template because the crystallizations of Mn + Zn into iron oxide form at lower temperature than firing of wood. Figure 3.22 summarizes the transformations process.

Sintered in air at the higher temperature, the hematites are remained. The Mn-Zn Fe_2O_4 was crystallized with α-Fe_2O_3 to form composite wood in higher temperatures. The

XRD pattern shows the XRD pattern for the infiltrated wood sintered in air with various sets of temperature and times. α-Fe_2O_3 peaks retained (figure 3.23). The entire patterns have a high count of hematite peak Fe_2O_3 ($2\theta = 33.2$) {h k l = 1 0 4}.
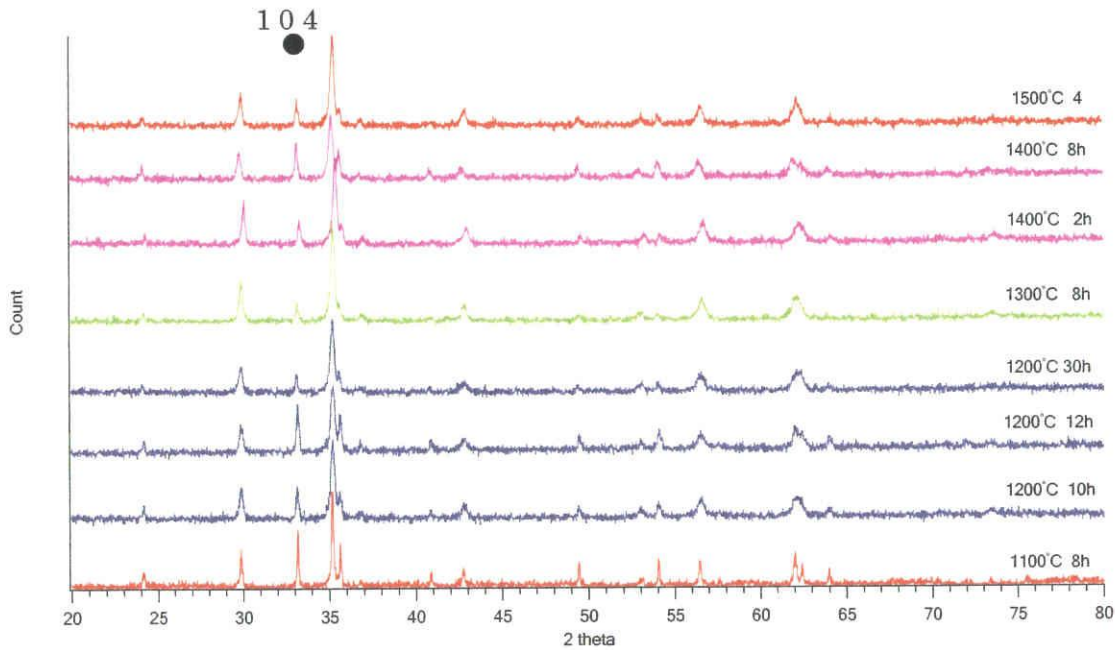

Figure 3.23 XRD pattern of Template sintered in air

As discussed earlier, sintering in air and sintering in argon atmosphere had been conducted in order to investigate the most suitable temperature, conditions and time h.

From the DT-TGA analysis, was found that it necessary to sintered the specimens in air for oxidation reaction of wood component. But it seems that, sintered in air unable to eliminate the $-Fe_2O_3$ peak. Some of the study suggests the sintering conditions of Mn-Zn ferrite must in free air conditions, because according [17], slowly cooled in N_2 atmosphere is necessary to prevent segregation of α-Fe_2O_4. Because of this reason the next attempt was conducted in air and final stage in Argon gas (section 2.2.4.2)

3.10   Single Phase $Mn_{0.5}Zn_{0.5}Fe_2O_4$

Figure 3.24 shows the XRD pattern for the Infiltrated template that sintered in air in earlier stage (Rt – 1200°C 6h) and in argon in final stage (1200°C 8h + 6 h cooling). The hematite peak was successfully eliminated and the entire higher peaks show the existence of typical spinel structure.
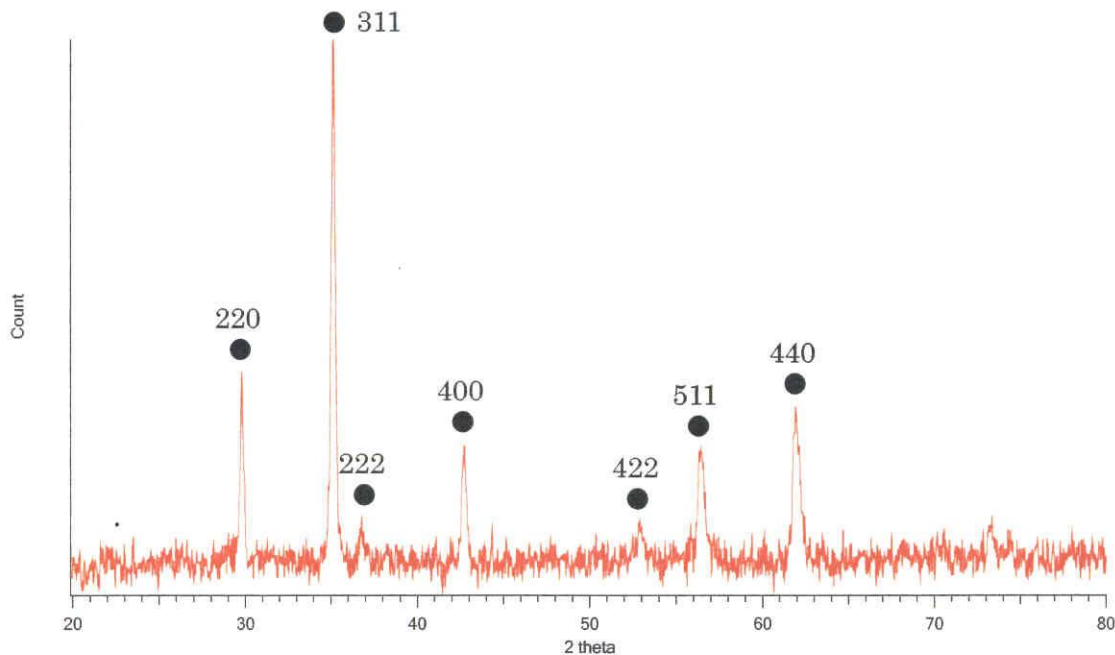

Figure 3.24 XRD pattern of $Mn_{0.5}Zn_{0.5}Fe_2O_4$ sintered at 8h in argon

3.10.1   XRD pattern of $Mn_xZn_{1-x}Fe_2O_4$ from wood template (X = 0.1,0.5 and 0.9)

The similar sintering conditions were conducted to produce the $Mn_xZn_{1-x}Fe_2O_4$ with different concentration of Mn^{2+}. The single phase Mn-Zn ferrites were obtained. Figure 3.25 shows the XRD pattern of $Mn_xZn_{1-x}Fe_2O_4$ for x = 0.1, 0.5 and 0.9. The peaks shifted to lower diffraction angles with increasing x. Since the ionic radius of Zn^{2+} (0.82 A) is smaller than that of Mn^{2+} (0.91 A) the lattice parameter become bigger (Fig.3.26)[48]. Each product with same concentration, x from different template showed the similar lattice constant in the range of ± 0.008Å. This argument was corresponded with the Jae-Gwang Lee et. Al (2006) that prepared Mn-Zn ferrite powder (figure 3.25).

The lattice constants differed from other report [48]. MnZn ferrite configuration based on a face- centered cubic lattice of oxygen ions with a unit cell consisting of 8 functional units. Spinel ferrite contains two types of sites, tetrahedral and octahedral sites. The Zn^{2+} ions had a marked preference for tetrahedral sites.
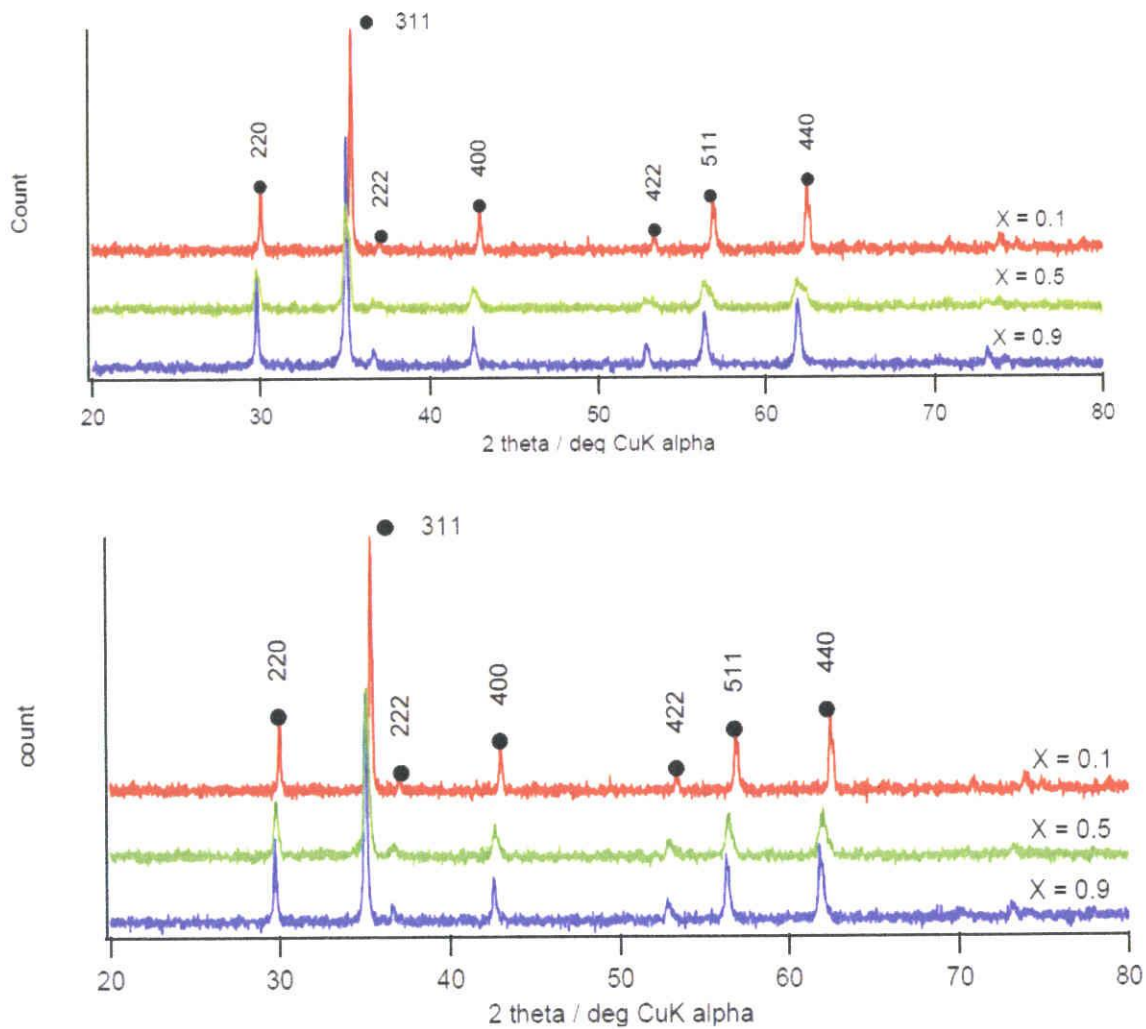

Figure 3.25 X- ray diffraction patterns of $Mn_xZn_{1-x}Fe_2O4$ sintered at 1200^oC in argon atmosphere (a.) from Cedar template (b.) from Balsa template

It confirms that, the mixed spinel ferrites were similar XRD pattern eventough prepared with different templates (cedar and balsa). This is because same condition was applied during sintering process.
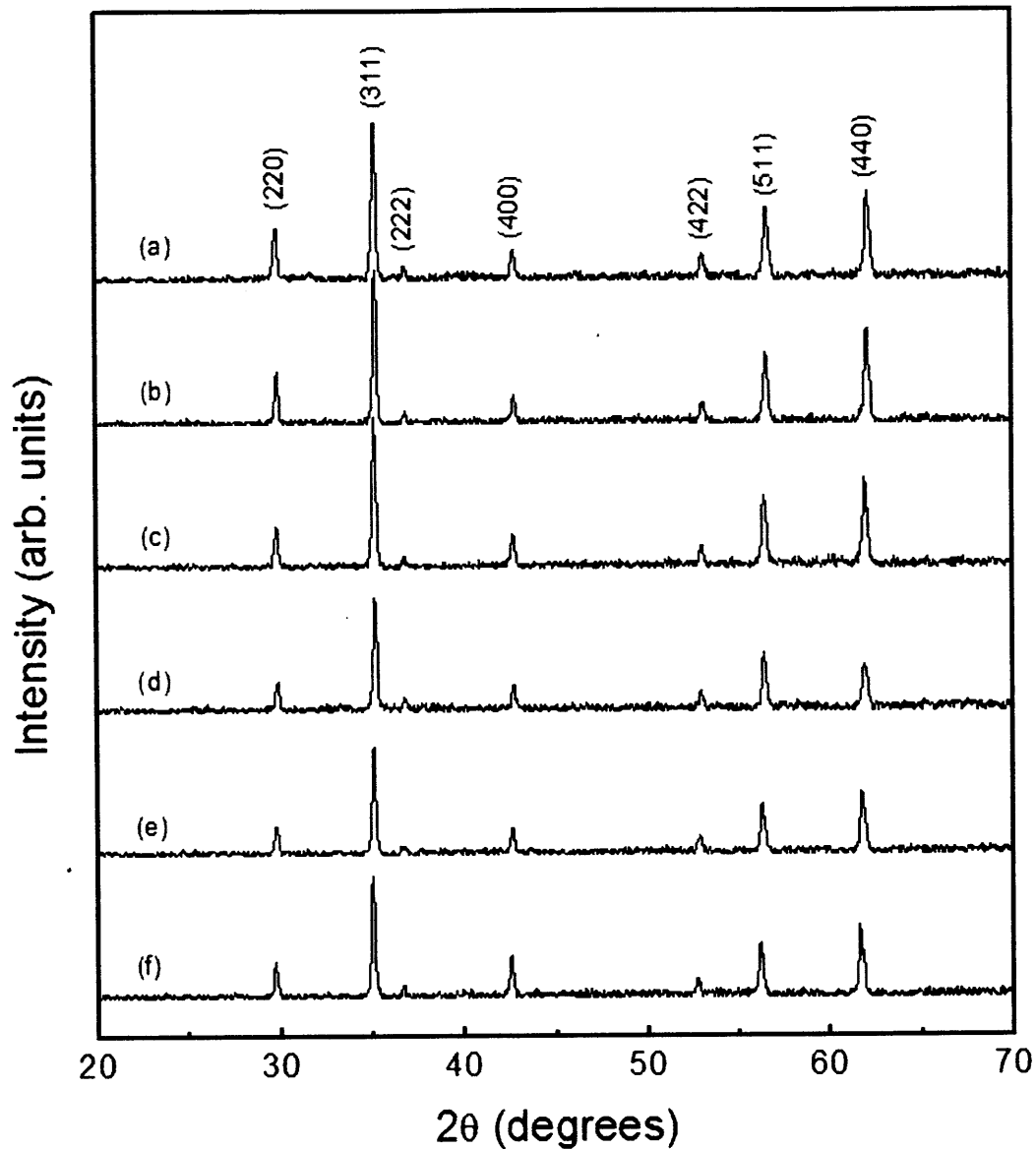
Figure 3.26 XRD patterns of $Mn_xZn_{1-x}Fe_2O_4$ powder (a) x = 0.0, (b) x = 0.2, (c) x = 0.4, (d) x =0.6, (e) x = 0.8, and (f) x = 1.0. Adapted from [48]

3.10.2 Lattice constant of Mn-Zn ferrite woods

Meanwhile figure 3.27 indicates the lattice constant of $Mn_xZn_{1-x}Fe_2O_4$; both sets of specimens perform a similar value of lattice. The lattice might slightly different due to the cation distribution depends on few factors, such as the temperature, pressure, compositions and preparation method [49]. At higher temperature, it leads to grain growth which affected the particle size as well as ionic distributions [17]. That caused

by some ion either Mn^{2+} or Zn^{2+} that occupied the tetrahedral and octahedral site of mixed spinel.

Table 3.9 The calculated lattice parameter of $Mn_xZn_{1-x}Fe_2O_4$ via XRD pattern

X = 0.1

2θ	d	i/i₀	h	k	l	a (Å)
30.02	2.973	54	2	2	0	8.409
35.38	2.534	100	3	1	1	8.404
37.02	2.425	39	2	2	2	8.401
42.98	2.102	47	4	0	0	8.407
53.34	1.715	40	4	2	2	8.404
56.86	1.617	50	5	1	1	8.404
62.44	1.485	55	4	4	0	**8.403**

X=0.5

2θ	d	i/i₀	h	k	l	a (Å)
29.78	2.996	59	2	2	0	8.475
35.1	2.553	100	3	1	1	8.469
36.74	2.443	45	2	2	2	8.463
42.6	2.120	51	4	0	0	8.478
52.94	1.727	45	4	2	2	8.463
56.48	1.627	55	5	1	1	**8.456**
61.98	1.495	56	4	4	0	**8.459**

X=0.9

2θ	d	i/i$_o$	h	k	l	a (Å)
29.74	3.00	54	2	2	0	8.486
35.02	2.55	100	3	1	1	8.487
36.62	2.45	35	2	2	2	8.490
42.54	2.127	43	4	0	0	8.490
52.78	1.73	37	4	2	2	8.486
56.26	1.63	50	5	1	1	8.486
61.78	1.49	53	4	4	0	**8.484**

Table 3.9 shows the calculated lattice for each peak for X = 0.1, 0.5 and 0.9. The different value of lattice was occurring due to the error of decimal point calculations and large angle change of 2θ. The lattice value at the largest angle was selected due to the lowest calculations error. Figure 3.26 conclude the lattice constant of the Mn$_x$Zn$_{1-x}$Fe$_2$O$_4$ (X = 0.1, 0.5 and 0.9) from wood templates.
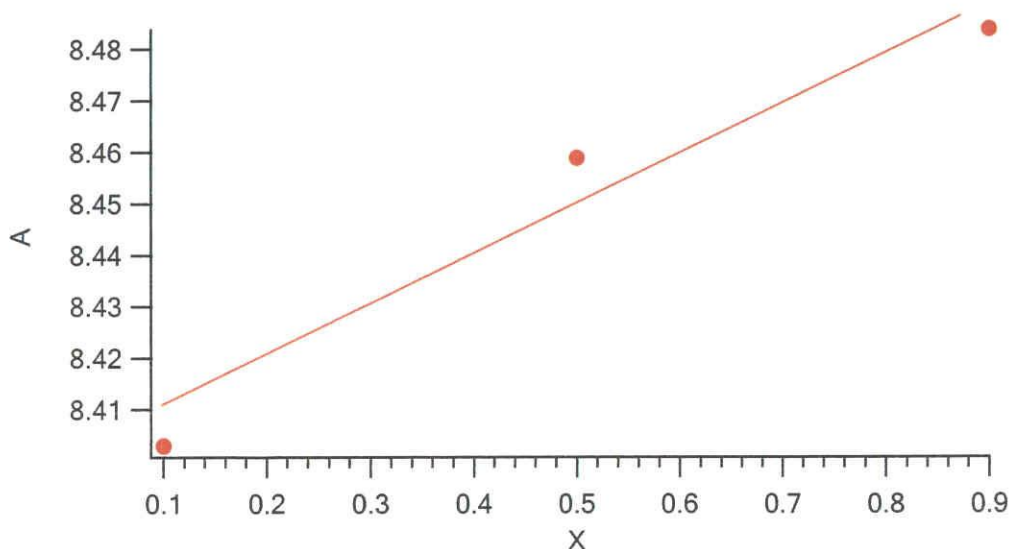

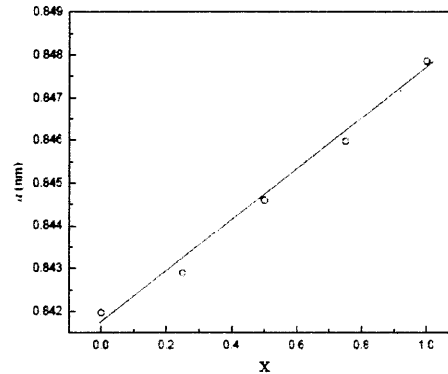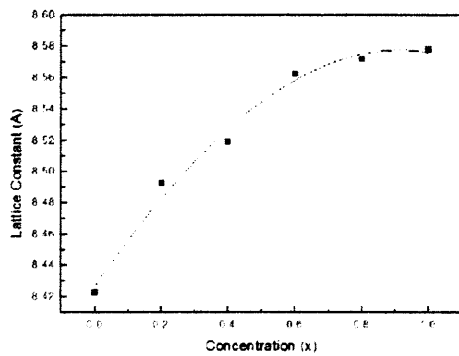Figure 3.27 Lattice constant as function of x for Mn$_x$Zn$_{1-x}$Fe$_2$O$_4$ from balsa and cedar

Fig. 2. Variation of the lattice constants of the Fig. (2): The variation of the lattice constant. a. with Mn^{2-} ions content.
$Zn_{1-x}Mn_xFe_2O_4$ ferrite powders.

Figure 3.28 Variation of lattice constant as function of x in $Mn_xZn_{1-x}Fe_2O_4$. (right) and (left) photo was adapted from [48] and [49] respectively.

The lattice constants obtained and reported [48] (fig 3.28 (left)) are much higher and not increase linearly by increasing of Mn^{2+}. This might be the ion inconstantly occupied at both hexahedral and octahedral sites. S.M Attia [49] (fig 3.28 (right)) reported the smaller lattice constant. All results shows the different lattice sizes, this might be due to the easiness of migrations of the ion to occupied both hexahedral and octahedral sites.

3.11   SEM of Mn-Zn Ferrite Wood

Figure 3.29 shows the microstructure of treated cedar wood. Meanwhile figure 3.30 illustrate the single phase Mn-Zn ferrite wood. In thus figure, it shows that most of wood shape retained. The sintered body was subtracted by array of 1 directional pores.
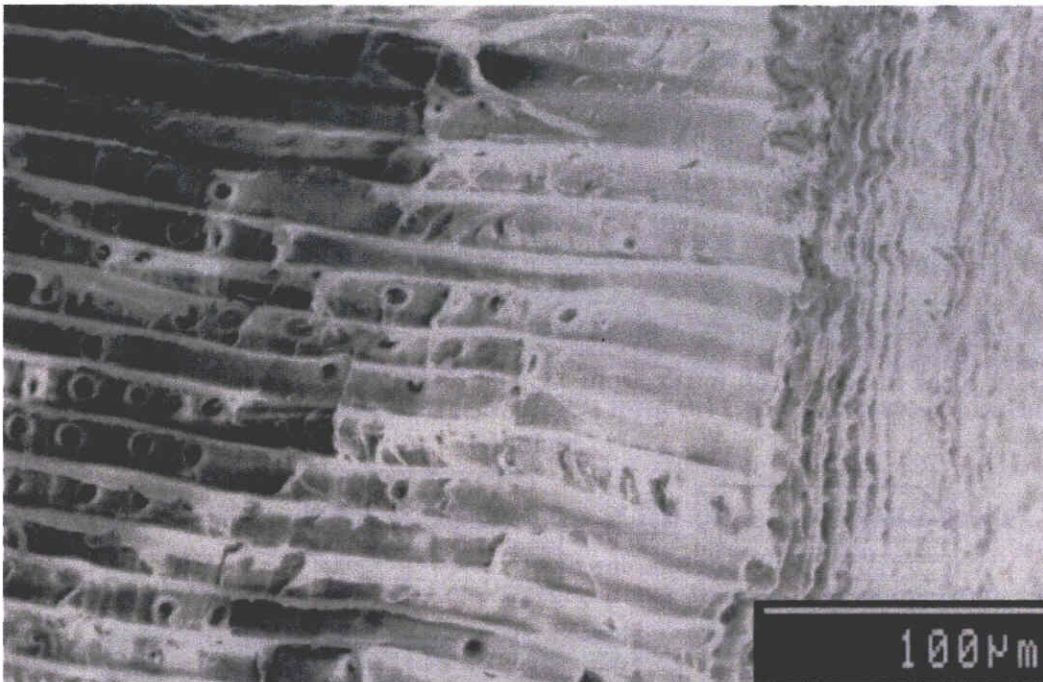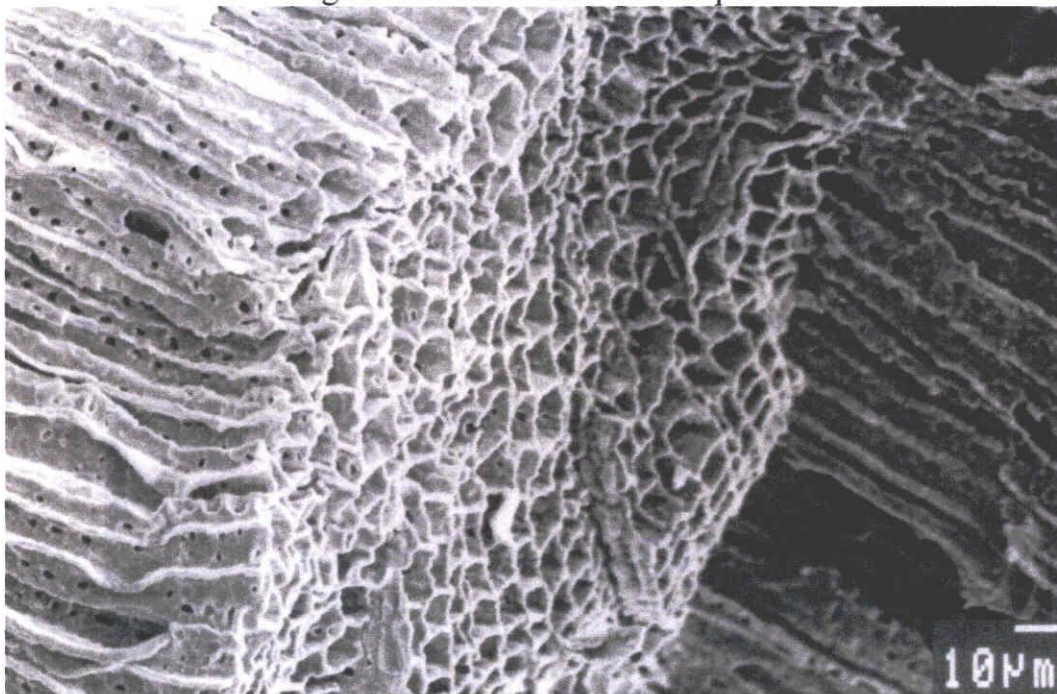
Figure 3.29 The cedar wood template

Figure 3.30 Ferrite wood (Mn-Zn ferrite)

Instead of cedar template, balsa template with bigger pores was used as template (figure 3.31). It seems like the Mn-Zn ferrite that mimicking balsa microstructure able to be obtained by similar process.
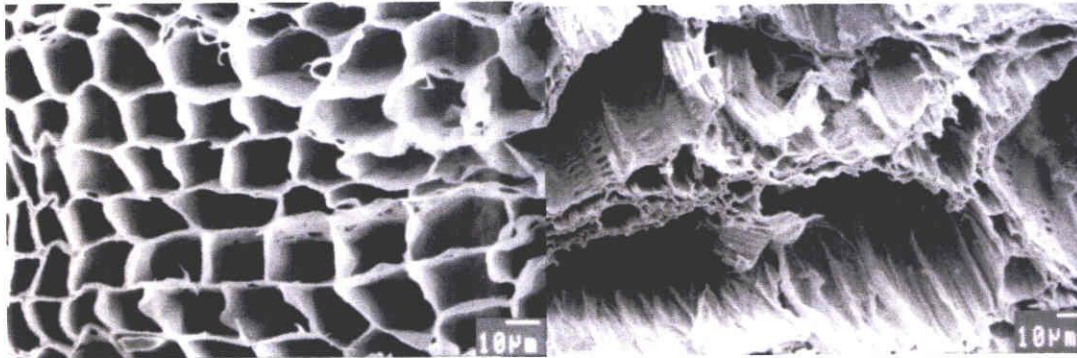
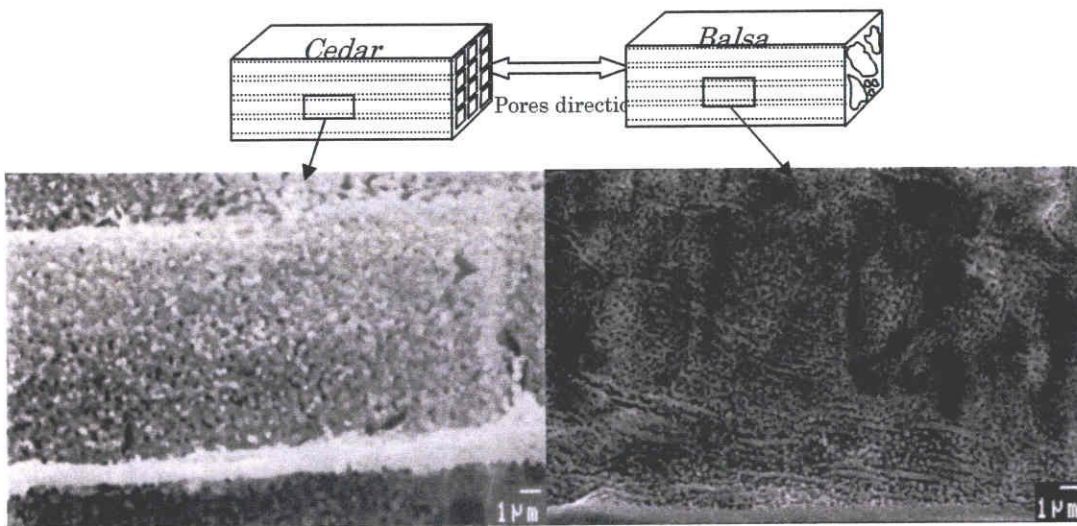Figure 3.31 SEM image MnZn ferrite from a.Cedar template, b.Balsa template.

Figure 3.32: Lateral image of $Mn_{0.1}Zn_{0.9}Fe_2O_4$ from (a) Cedar template (b) Balsa template.
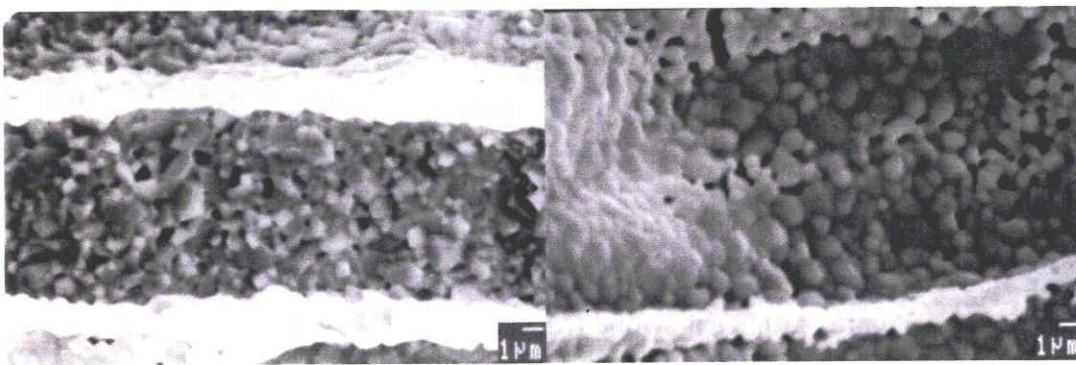

Figure 3.33: Lateral image of $Mn_{0.5}Zn_{0.5}Fe_2O_4$ from (a) Cedar template (b) Balsa template.
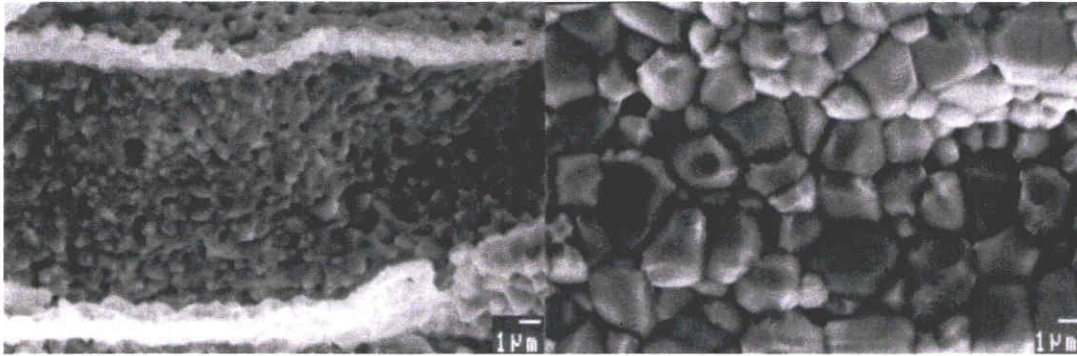
Figure 3.34 Lateral image of $Mn_{0.9}Zn_{0.1}Fe_2O_4$ from (a) Cedar template (b) Balsa template.

Figure 5 shows typical microstructures of ferrite woods (Mn-Zn ferrite). The product from *Balsa* template had much larger pores than that product from *Cedar* template. Their pore sizes were approximately (50 x 20) μm^2 and (15 x 15) μm^2 respectively shown in Figure 3.31. The shape of pores was retained, where the pores elongated in one direction. For the case of rich Zn^{2+}, the pores were smallest because of the grain were growth bigger.

3.12   Grain sizes of Mn-Zn Ferrite Wood

Figures 3.31, 3.32 and 3.33 shows lateral images of the $Mn_xZn_{1-x}Fe_2O_4$ (x = 0.1, 0.5 and 0.9). For x = 0.1 both products were composed of fine grains. The grain grew up with increasing of Mn concentration. Especially, $Mn_{0.9}Zn_{0.1}Fe_2O_4$ from *Balsa* template showed an extraordinary grain growth. Probably, it is caused by impurity containing in *Balsa* wood.

3.13   Ba-ferrite

Ba- ferrites with the hexagonal crystal structure were studied. This M-type hexagonal ferrites that mimicked wood microstructure was produced. The preparations approach was determined. $BaFe_{12}O_{19}$ have a theoretical density 5.28 g/cm^3 [16].

3.13.1 DT-TGA of infiltrated template

Figure 3.35 shows the DT-TGA of infiltrated templates. The wood template that infiltrated with the (Ba nitrate, Iron nitrate and citric acid) precursor solutions (table 2.3 Chapter 2) was crush into powder and the DT-TG was examined. The results consisted few exothermic peaks. First phase endothermic peak (~ $100^{\circ}C$) due to the removal of wet or dehydration. The transformation process similar with the NiZn-ferrite and MnZn ferrite which is the decompositions of mixed starting material (Ba nitrate + Fe nitrate) was occurred around ~$130^{\circ}C$-$160^{\circ}C$. Then followed by the decompositions of wood component around $260^{\circ}C$ (similar transformation as NiZn ferrite wood). The exothermic peak at $360^{\circ}C$ represents the crystallizations of the Mixed Ba nitrate and Fe nitrate into Oxide form. And finally the wood component was removed around $510^{\circ}C$.
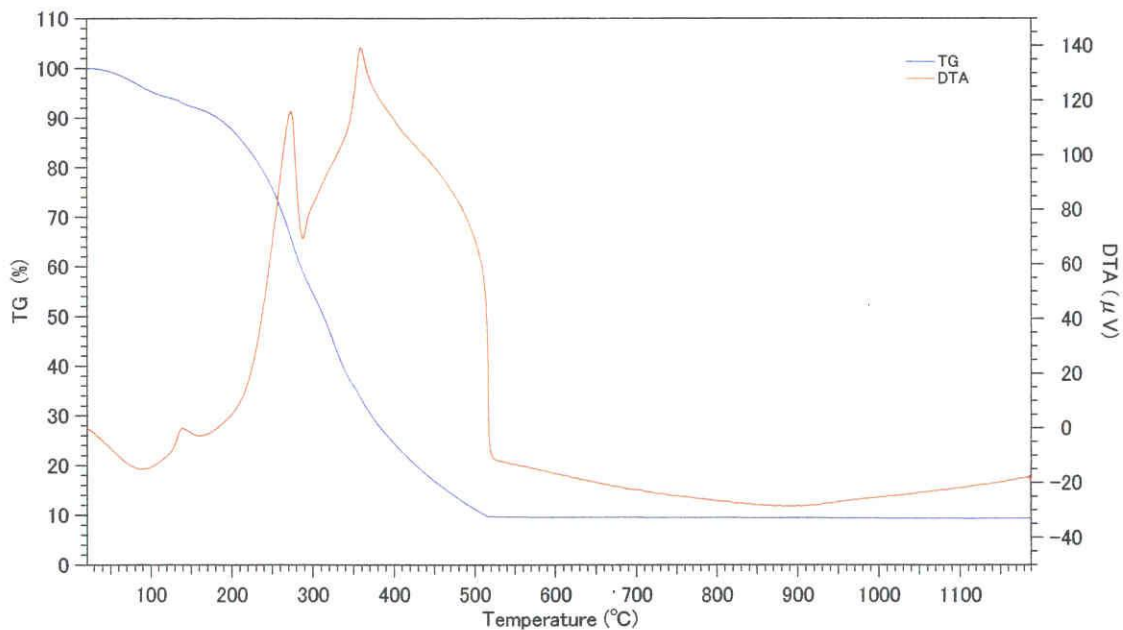

Figure 3.35 TG, DTA recorded at $10^{\circ}C$/min of cedar wood

Figure 3.36 summarized the transformations of infiltrated wood into Ba-ferrite wood.
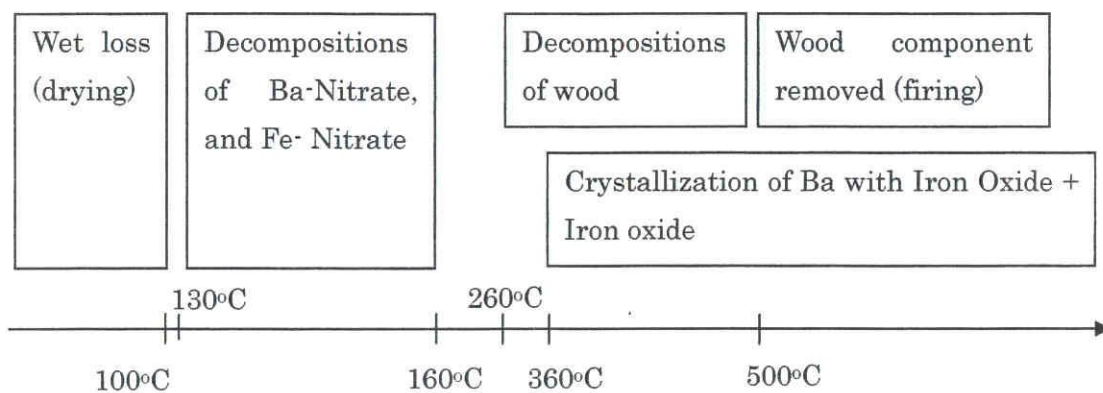
Figure 3.36 Summarize the transformations process of infiltrated woods into ferrite wood
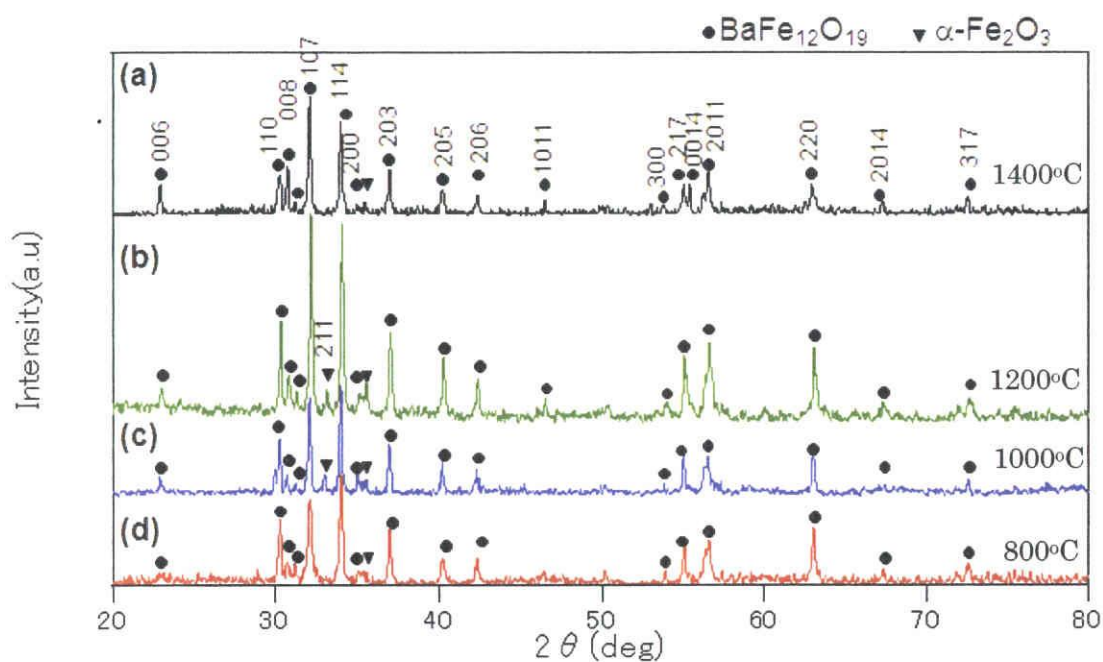
3.13.2 XRD pattern of Ba-ferrite wood

Figure 3.37 XRD pattern of Infiltrated wood sintered at $800^{\circ}C - 1400^{\circ}C$.

Figure 3.37 shows the XRD pattern of infiltrated template that sintered at $800^{\circ}C$, $1000^{\circ}C$, $1200^{\circ}C$ and $1400^{\circ}C$. The results indicated the weak peak of hematite

was revealed at all temperature. But at 1200°C the (1011) peak was form. Meanwhile the complete set of $BaFe_{12}O_{19}$ peak was form at 1400°C which is the peak (0014) was revealed and the hematite peak was almost eliminated. This agrees with [15, 52] that the typical reaction temperature for hexagonal ferrite is as high as 1450°C because of their complex structures.

3.13.3 Ba-ferrite woods at higher temperature.

3.13.3.1 Physical and color

Similar with NiZn ferrite and MnZn ferrite, the woody microstructure of Ba-ferrite was defected at higher temperature due to the shrinkages. The figure shows the Ba-ferrite wood that sintered at 800°C – 1400°C. It shows the changes of the color form brown to grey because of amount hematite lesser at higher temperature. This corresponded with the color of hematite is red or brown and the color of ferrite is black. Instead the XRD pattern indicated the similar phenomenon too.
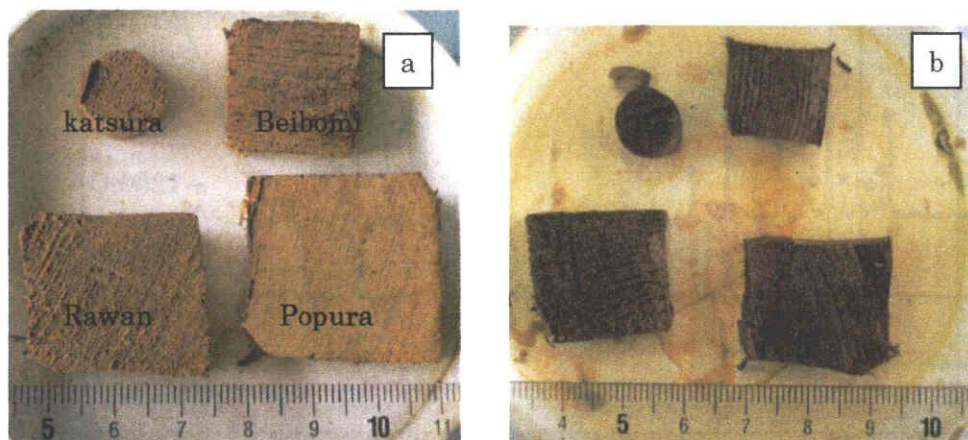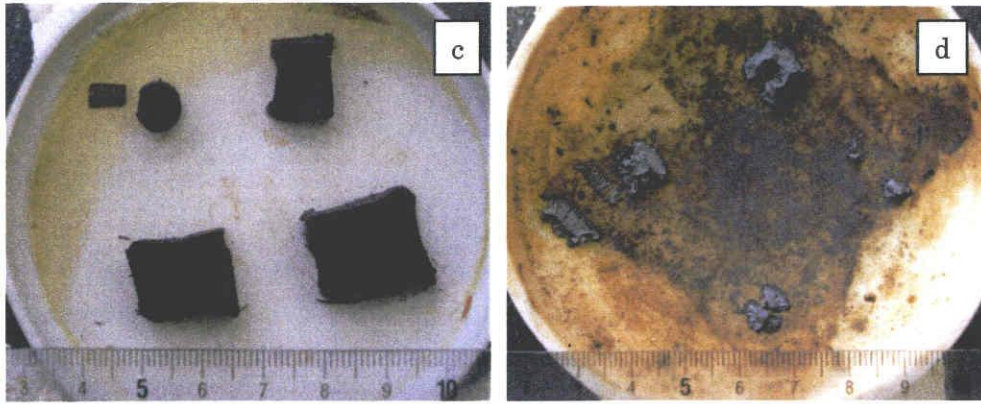
Figure 3.38: 4 different type of wood template (a) Original infiltrated templates (b) sintered at 800°C (c) sintered at 1000°C and (d) sintered at 1200°C

Sintered at 800°C the shape retained in good conditions. By increased to 1000°C the ferrite wood shape was defected and at 1200°C the specimen was highly shrinks and cracked and the color becomes dark (figure 3.38). Finally at 1400°C the specimens aren't in woody shape. As a conclusions single phase Ba-ferrite are crystallized at 1450°C [15, 52] but the woody shape unable to retained at such high temperature due to the high shrinkages.

3.13.3.2 Shrinkages

Table 3.10 shows the shrinkages of the Ba-ferrite wood that sintered at 800°C and 1000°C. The results show that the specimens from *Katsura* template have a largest shrink. This is because *Katsura* template consist the biggest pores approximately 50μm. The ferrite wood from *Beibomi*, *Rawan* and *Popura* template have almost similar shrinkages. This might be due to the similar pores sizes (~10 μm). Sintered at 1400°C the specimens was totally deform into non-woody shape microstructures.

Table 3.10 sintered size/template size of Ba-ferrite wood under different sintering temperature

Template	Sintered temperature 800°C	Sintered temperature 1000°C
Katsura	0.79	0.57

77

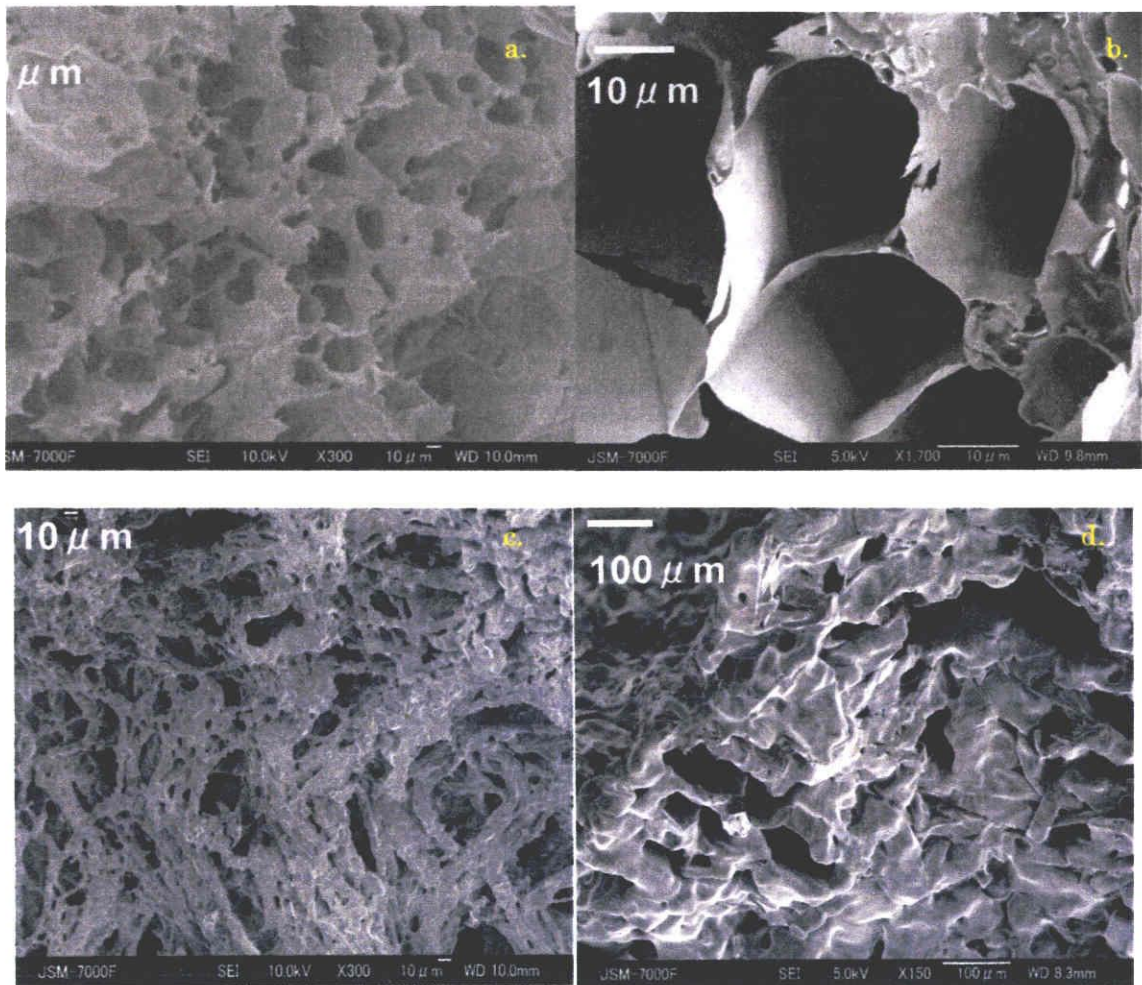|		
Beibomi	0.83	0.6
Rawan	0.83	0.59
Popura	0.83	0.59

3.13.4   SEM of Ba- Ferrite

Figure 3.39, sintered infiltrated wood at (a) 800°C, (b) 1000°C, (c) 1200°C and (d) 1400°C

Figure 3.39 shows the SEM images of the Ba-ferrites wood. Thus images confirm that sintered at 800°C and 1000°C the wood microstructure retained. Meanwhile at 1200°C only partial wood microstructure retained. But at 1400°C non-

78

wood microstructure was revealed. In additions of that, the grains sizes were growth by increasing of sintering temperature.

3.13.4.1 Grain sizes of Ba-ferrite wood

The crystallizations of Ba-ferrite occurred at high temperature. The grain size growth began at 1000°C onward. Instead of Ba-ferrite, α- Fe_2O_3 was also revealed. But according to the XRD, the phase of α- Fe_2O_3 become lesser at higher sintering temperatures. The grains size was growth rapidly at 1000°C – 1200°C and 1200°C – 1400°C (table 3.11). The higher sintering temperature caused contraction among the pores and no wood microstructure retained.

Table 3.11 shows the approximations of the grain sizes sintered at various temperatures.

Sintering temperature, °C	Grain sizes, μm	Conditions	Phase exist
800	< 1 μm	Wood microstructure retained	$BaFe_{12}O_{19}$ +α-Fe_2O_3
1000	< 1 μm	Wood microstructure retained	$BaFe_{12}O_{19}$ +α-Fe_2O_3
1200	~ 7- 10 μm	Wood microstructure partially retained	$BaFe_{12}O_{19}$ +α-Fe_2O_3
1400	> 20 μm	No wood microstructure retained	$BaFe_{12}O_{19}$ +α-Fe_2O_3

The single phase Ba-ferrite wood unsuccessfully prepared. This is because the single phase Ba-ferrite was completely crystallized at 1450°C. That temperature was too high for the woody microstructure to retain. In can be confirmed by the grain sizes at 1400°C that approximately 20 – 30 μm which is larger than the expected pores size.